

Analysis of meiosis in *Pristionchus pacificus* reveals plasticity in homolog pairing and synapsis in the nematode lineage

Regina Rillo-Bohn^{1,2,3,4}, Renzo Adilardi^{1,2,3,4}, Barış Avşaroğlu^{1,2,3,4}, Lewis Stevens⁵, Simone Köhler^{1,2,3,4,6}, Joshua Bayes^{1,2,3,4}, Clara Wang^{1,2,3,4}, Sabrina Lin^{1,2,3,4}, Kayla Baskevitch^{1,2,3,4}, Abby F. Dernburg^{1,2,3,4}

¹Department of Molecular and Cell Biology, University of California, Berkeley, Berkeley, CA United States; ²Howard Hughes Medical Institute, Chevy Chase, MD United States; ³Biological Systems and Engineering Division, Lawrence Berkeley National Laboratory, Berkeley, CA United States; ⁴California Institute for Quantitative Biosciences, Berkeley, CA United States; ⁵Institute of Evolutionary Biology, University of Edinburgh, Edinburgh, UK; ⁶Cell Biology and Biophysics Unit, European Molecular Biology Laboratory, Heidelberg, Germany

1 **ABSTRACT**

2 Meiosis gives rise to haploid gametes from diploid progenitor cells. Here we describe a new,
3 comparative model system for molecular analysis of meiosis, the nematode *Pristionchus*
4 *pacificus*, a distant relative of the widely studied model organism *Caenorhabditis elegans*.
5 Despite superficial similarities in germline organization and meiotic progression between *P.*
6 *pacificus* and *C. elegans*, we identify fundamental differences in the molecular mechanisms
7 underlying homolog pairing, synapsis, and crossover regulation. Whereas *C. elegans* has lost
8 the meiosis-specific recombinase Dmc1, *P. pacificus* expresses both DMC-1 and RAD-51, which
9 localize sequentially to meiotic chromosomes during prophase. *Ppa-spo-11* and *Ppa-dmc-1* are
10 required for stable homolog pairing, synapsis, and crossover formation, while *Ppa-rad-51* is
11 dispensable for these key processes during early prophase. Additionally, we show that
12 elevated crossover recombination in *P. pacificus* likely arises through a Class II pathway
13 normally inactive in *C. elegans*, shedding light on crossover control and the evolution of
14 recombination rates.

15

16 INTRODUCTION

17 All sexually reproducing organisms rely on the specialized cell division process of
18 meiosis to generate haploid gametes from diploid precursors. Upon fertilization, haploid
19 gametes fuse and restore the diploid chromosome complement in the zygote. Thus, meiosis is
20 essential for the survival of sexually reproducing species. This process was likely present in the
21 last eukaryotic common ancestor (LECA). Studies in plants, animals, fungi, and protists have
22 revealed intriguing diversity in the details of meiotic mechanisms.

23 A defining feature of meiosis is a “reductional” segregation in which homologous
24 chromosomes are separated, usually during the first of two nuclear divisions. A highly
25 choreographed series of chromosome transactions precedes this division and ensures faithful
26 homolog segregation: (1) pairing, in which chromosomes contact and recognize their
27 homologous partners; (2) synapsis, defined as the assembly of a protein ensemble called the
28 synaptonemal complex (SC) between homologs, which leads to their lengthwise alignment;
29 and (3) crossover (CO) recombination, which creates physical linkages between chromosomes
30 that promote proper bi-orientation during anaphase I. Failure to form at least a single CO
31 between paired homologs results in nondisjunction and aneuploid gametes (Zickler and
32 Kleckner, 1999).

33 Although homolog pairing, synapsis and CO recombination during meiosis are nearly
34 ubiquitous among eukaryotes, key aspects of these chromosomal transactions show
35 remarkable diversity among different lineages. In most model fungi, plants, and animals,
36 stable homologous chromosome pairing and synapsis depend on early steps of the

37 recombination pathway. Meiotic recombination is initiated by a conserved topoisomerase-like
38 enzyme called Spo11, which catalyzes programmed DNA double-strand breaks (DSBs) across
39 the genome, a subset of which are ultimately processed into COs (Keeney, 2008; Keeney et al.,
40 1997). DSBs are resected to form 3' single-stranded DNA overhangs. Dmc1, a meiosis-specific
41 recombinase, forms filaments along the resulting ssDNA segments and promotes
42 interhomolog strand invasion. Rad51 is often required as a cofactor for these early steps in
43 recombination. Spo11-dependent induction of DSBs and Dmc1-dependent strand invasion are
44 crucial for stable homolog pairing and synapsis in the budding yeast *Saccharomyces cerevisiae*,
45 the flowering plant *Arabidopsis thaliana*, and mammalian model *Mus musculus* (Bishop et al.,
46 1992; Couteau et al., 1999; Grelon, 2001; Pittman et al., 1998; Rockmill et al., 1995; Yoshida et
47 al., 1998).

48 In contrast, recombination-independent mechanisms of pairing and synapsis have been
49 characterized in other prominent model systems, including the dipteran *Drosophila*
50 *melanogaster* and the nematode *Caenorhabditis elegans*. While recombination is essential for
51 successful execution of meiosis in *C. elegans* and in female fruit flies, homolog pairing and
52 synapsis can be uncoupled from early recombination events. In the female germline of *D.*
53 *melanogaster*, homolog pairing initiates in proliferating germline stem cells even before they
54 enter meiosis (Christophorou et al., 2013; Joyce et al., 2013; Rubin et al., 2016) and is stabilized
55 by SC formation during early prophase. *D. melanogaster* males lack recombination and SCs,
56 and have apparently evolved a distinct mechanism to stabilize homolog pairing and enable
57 reductional segregation (McKee et al., 2012). In *C. elegans*, pairing and synapsis are driven by
58 Pairing Centers, specialized sites on each chromosome bound by a family of zinc-finger

59 proteins that mediate nuclear envelope attachment and chromosome dynamics (MacQueen et
60 al., 2005; Phillips et al., 2005; Phillips and Dernburg, 2006; Sato et al., 2009). While nuclear
61 envelope attachment and chromosome movement play important roles in meiotic pairing and
62 synapsis across eukaryotes, in *C. elegans* they have acquired a critical role in coupling homolog
63 pairing to synapsis initiation (Penkner et al., 2009; Sato et al., 2009).

64 To investigate how the meiotic program is modified during evolution, we have
65 established tools to investigate meiosis in the free-living nematode *Pristionchus pacificus*. Like
66 its distant relative *C. elegans*, *P. pacificus* is an androdioecious species, characterized by a
67 population of mostly self-fertilizing hermaphrodites (XX) and a low frequency of males (XO)
68 (Sommer et al., 1996). Like *C. elegans*, *P. pacificus* has a short life cycle of 3.5 days, produces
69 large broods of about 200 progeny by self-fertilization, and is easily cultured in the lab (Hong
70 and Sommer, 2006). Although *C. elegans* and *P. pacificus* diverged an estimated 200-300
71 million years ago (Pires-daSilva, 2004), they share the same number of chromosomes ($2n=12$)
72 and, with the exception of one major chromosomal translocation, macrosynteny is maintained
73 between the two species (Dieterich et al., 2008; Rödelsperger et al., 2017). *P. pacificus* has been
74 established as a model for comparative studies in development, evolution and ecology
75 (Sommer, 2015). Recent improvements in the genome assembly (Rödelsperger et al., 2017)
76 and advances in genome editing (Lo et al., 2013; Namai and Sugimoto, 2018; Witte et al., 2015)
77 have facilitated investigation of cell biological processes at a more mechanistic level.

78 In addition to these general features that make *P. pacificus* a tractable model system,
79 previous studies have suggested interesting differences from *C. elegans*. First, genome
80 sequencing revealed the presence of the Dmc1 gene, which is absent from the entire

81 *Caenorhabditis* clade (Figure 2 - Supplement 1 and Dieterich et al., 2008). Loss of Dmc1
82 correlates with the adaptation of recombination-independent mechanisms for pairing and
83 synapsis in *Drosophila* and *Caenorhabditis* (Villeneuve and Hillers, 2001). Therefore, it was of
84 great interest to us to examine how homologous chromosomes pair and synapse in the
85 presence of Dmc1. Second, genetic linkage maps have revealed that multiple COs typically
86 occur per chromosome pair during meiosis in *P. pacificus* (Srinivasan et al., 2003, 2002). This is
87 in striking contrast to *C. elegans*, which exhibits complete CO interference; only a single Class I
88 CO normally occurs per chromosome pair (Martinez-Perez and Colaiácovo, 2009). These
89 observations suggest a major difference in the mechanism of CO control between these two
90 species.

91 By employing CRISPR/Cas9-mediated genome editing techniques, genetics,
92 immunocytochemistry and microscopy, we describe here the early events of meiotic prophase
93 in *P. pacificus*. We show that homolog pairing, synapsis and CO recombination are dependent
94 on *Ppa-spo-11* and *Ppa-dmc-1*, while *Ppa-rad-51* is not essential for meiosis. We also provide
95 evidence that a single Class I CO occurs per homolog pair in *P. pacificus*, implying that the
96 higher recombination rate is due to Class II COs. Our work establishes tools for future
97 investigation and highlights the flexibility of the meiotic program within the nematode lineage.

98

99 **RESULTS**

100 ***P. pacificus* as a comparative model system for meiosis**

101 The morphology and organization of the *P. pacificus* germline is very similar to that of
102 *C. elegans*. Hermaphrodites have two gonad arms in which sperm and ova are produced

103 sequentially, while males have a single arm (Rudel et al., 2005). The switch from
104 spermatogenesis to oogenesis occurs during early adulthood. DAPI staining of adult
105 hermaphrodite gonads reveals a cylindrical monolayer of cells; the distal tip is populated by
106 proliferating germline stem cells (Figure 1A-C). As germ cells enter meiosis, their nuclear
107 morphology abruptly becomes asymmetrical, as the chromosome mass adopts a conspicuous,
108 crescent-shaped morphology (Figure 1A). Immediately proximal to this “transition zone,” DAPI
109 staining reveals parallel tracks, indicative of paired and synapsed homologous chromosomes at
110 the pachytene stage. Oocyte chromosomes in *P. pacificus* undergo a dramatic decondensation
111 between diplotene and diakinesis, a stage that has been referred to as the “growth zone”
112 (Rudel et al., 2005) or “diffuse stage” (Zickler and Kleckner, 1999). Similar diffuse chromosome
113 morphology is observed during late prophase in other eukaryotes, but is rarely seen in *C.*
114 *elegans*. As oocytes mature in the proximal region of the hermaphrodite gonad, they form a
115 single row of large cells, and chromosomes condense dramatically as the nuclei grow in size.
116 Six bivalents can be detected as compact DAPI-staining bodies during diakinesis, the stage
117 preceding the first meiotic division, during oogenesis (Figure 1A, Sommer et al., 1996, Rudel et
118 al., 2005).

119 It has been assumed that chromosomes in *P. pacificus* are holocentric, as in *C. elegans*,
120 but we are unaware of direct evidence to support this idea. We thus identified a gene encoding
121 CENP-C (HCP-4 in *C. elegans*), a conserved kinetochore protein, in the *P. pacificus* genome and
122 inserted a V5 epitope tag at its 3' end using CRISPR/Cas9. The appearance of mitotic
123 chromosomes in embryos and in the premeiotic germline confirmed their holocentric

124 organization (Figure 1C). Ppa-CENP-C::V5 forms linear structures, a hallmark of holocentric
125 chromosomes, instead of discrete foci as observed for monocentric chromosomes.

126

127 **Stable homolog pairing requires early recombination factors**

128 BLAST searches of the *P. pacificus* genome revealed an open reading frame encoding
129 an unambiguous ortholog of Dmc1, a meiosis-specific paralog of Rad51 (Table S1). An ortholog
130 of the Dmc1 cofactor Mnd1 was also readily identified; although its partner Hop2 was not
131 apparent among the predicted proteins or published nucleotide sequence (Figure 2 –
132 Supplement 1). By contrast, Dmc1/Mnd1/Hop2 are absent from both *C. elegans* and *D.*
133 *melanogaster*, two model organisms that have evolved recombination-independent
134 mechanisms of homolog pairing and synapsis (Villeneuve and Hillers, 2001). We analyzed the
135 genome sequences of other nematodes to determine the evolutionary history of these genes
136 within the nematode lineage (Bolt et al., 2018; <https://parasite.wormbase.org>). This analysis
137 revealed that Dmc1/Mnd1/Hop2 have been lost several times during the evolution of
138 nematodes, including the entire *Caenorhabditis* genus and all sequenced members of Clade IV
139 (Figure 2 –Supplement 1). Not surprisingly in light of its essential function in DNA repair, the
140 recombinase Rad51 was detected in almost all genomes with the exception of *Haemonchus*
141 *contortus*, *Parascaris univalens* and *Parascaris equorum* (data not shown). It is likely that the
142 absence of Rad51 orthologs reflects incomplete genome assembly and/or annotation in these
143 species.

144 Our analysis also identified homologs of four related zinc finger proteins required for
145 pairing center activity in *C. elegans* (HIM-8, ZIM-1, ZIM-2, and ZIM-3) in most of the genome

146 sequences from Clade V. Thus, many species within this clade have genes encoding both
147 pairing center proteins and Dmc1/Mnd1/Hop2, but *Caenorhabditids* have lost the latter while
148 *Pristionchus* apparently diverged before the emergence of the former.

149 We tested whether homolog pairing in *P. pacificus* is dependent on these early
150 recombination factors. To generate *spo-11*, *dmc-1* and *rad-51* null mutants, we employed
151 TALEN-mediated gene disruption, and later CRISPR/Cas9 genome editing techniques (this
152 study; Lo et al., 2013; Witte et al., 2015). Methods such as co-CRISPR that facilitate detection
153 of genome editing events in *C. elegans* have not been helpful for *P. pacificus* in our hands or
154 others' (Witte et al., 2015, and data not shown). Nevertheless, we were able to isolate mutant
155 alleles by screening a large number of F1 progeny from injected hermaphrodites (see Materials
156 and Methods). Independent alleles isolated from either TALEN or CRISPR-mediated genome
157 editing resulted in identical mutant phenotypes. All data presented here were based on alleles
158 generated by CRISPR/Cas9. Because balancer chromosomes are not currently available for *P.*
159 *pacificus*, most mutations described here were maintained in unbalanced heterozygotes, which
160 were identified by PCR-based genotyping. Self-fertilization of heterozygotes results in broods
161 with 25% homozygous mutant animals.

162 As expected, disruption of either *spo-11* or *dmc-1* resulted in the detection of 12 DAPI-
163 staining univalent chromosomes at diakinesis, indicative of a failure in CO recombination
164 (Figure 5). Surprisingly, *rad-51* mutants showed only mild meiotic defects (see below), and we
165 thus validated the loss of RAD-51 function in mutant animals by generating multiple alleles
166 that showed indistinguishable phenotypes, and also confirmed the absence of RAD-51 protein
167 by immunofluorescence with a polyclonal antibody against Ppa-RAD-51 (Figure 4 –

168 Supplement 1A, see Materials and Methods). Mutations in *spo-11* or *dmc-1*, but not *rad-51*, also
169 resulted in an obvious extension of the region of the germline displaying the crescent-shaped
170 nuclear morphology characteristic of early meiosis (Figure 2 – Supplement 2). A similar
171 “extended transition zone” phenotype is seen in *C. elegans* mutants that fail to synapse their
172 chromosomes during meiosis, suggesting that *spo-11* and *dmc-1* might be required for synapsis
173 in *P. pacificus*.

174 To visualize and quantify homolog pairing, we generated FISH probes against two short
175 tandem repeats found on Chromosome X and IV (Figure 2A). We measured the distance
176 between pairs of homologous FISH signals in individual nuclei for each genotype. To analyze
177 pairing kinetics, we divided the distal gonads into five zones of equal length. In zone 1, which
178 mostly consists of proliferating germ cells, pairs of FISH signals remained far apart, with an
179 average distance of $2.4 \pm 1.0 \mu\text{m}$ (SD) and $2.5 \pm 0.8 \mu\text{m}$ for Chrom X and IV, respectively (Figure
180 2B, D). In zone 2, which spans the transition zone, the average distances decreased
181 significantly in wild-type animals ($1.2 \pm 1.1 \mu\text{m}$ and $1.1 \pm 1.1 \mu\text{m}$ for Chrom X and IV,
182 respectively), and homologous signals remained closely associated in the subsequent meiotic
183 stages. Notably, homologous FISH probes localized closer together, on average, in the two
184 zones immediately following meiotic entry, and showed some separation in zones 4 and 5
185 (Figure 2B, D). By contrast, in wild-type *C. elegans*, homologous loci remain closely apposed in
186 most of the distal region of the gonad (MacQueen et al., 2002). Together with analysis of
187 synapsis (below), this indicated that desynapsis initiates shortly after completion of synapsis in
188 *P. pacificus*, resulting in partial separation of homologs.

189 We noted that the average distances between pairs of homologous FISH signals in *spo-*
190 *11* and *dmc-1* mutants also decreased markedly upon meiotic entry, although clearly less so
191 than in wild type (Figure 2D). In contrast, *rad-51* mutants showed distributions of probe
192 distances similar to wild-type animals (Figure 2C, D). We considered the possibility that the
193 proximity between FISH signals might reflect the clustering of all chromosomes within a
194 subregion of the nucleus, which is apparent during the “transition zone” (leptotene/zygotene),
195 rather than specific homologous interactions. If so, the extended transition zone morphology
196 in *spo-11* and *dmc-1* might obscure a pairing defect that would be more apparent in the
197 absence of clustering (Figure 2 – Supplement 2). To address this, we measured the distances
198 between pairs of heterologous FISH signals in the premeiotic region (dispersed) versus the
199 transition zone (clustered). We observed that heterologous FISH signals were also significantly
200 closer to each other in the transition zone compared to premeiotic nuclei in both wild-type and
201 mutant animals (Figure 2E). Furthermore, the distances between heterologous versus
202 homologous pairs of FISH loci were not significantly different in *spo-11* and *dmc-1* mutants
203 ($p=0.1777$ and $p=0.6774$, respectively, by Student’s *t*-test), but were clearly different in wild-
204 type meocytes ($p<0.0001$ by Student’s *t*-test) (Figure 2E). These data support the idea that
205 clustering, rather than specific pairing, promote proximity between both homologous and
206 heterologous loci during leptotene/zygotene in *spo-11* and *dmc-1* mutants. Although we
207 cannot conclude that transient homologous pairing is absent in these mutants, it is evident
208 that these early recombination factors are required for stable pairing and extended association
209 of homologous loci throughout prophase. In contrast, *rad-51* is dispensable for homolog
210 pairing, as in *C. elegans*.

211

212 **SPO-11 and DMC-1 are required for homologous synapsis**

213 To further investigate meiotic progression in *P. pacificus* and to probe the role of early
214 recombination factors in synapsis, we developed cytological markers for the chromosome axis,
215 which normally assembles upon meiotic entry, and the synaptonemal complex (SC), which
216 assembles between paired axes during early prophase. Identification of a candidate axial
217 element component was straightforward, due to the presence of the easily recognized
218 HORMA (Hop1, Rev7, Mad2) domain among members of this family of proteins (Aravind and
219 Koonin, 1998; Vader and Musacchio, 2014). We identified a gene encoding a HORMA domain
220 protein that is most closely related to *Cel-him-3* by reciprocal BLAST analysis (Table S1). We
221 refer to this protein as Ppa-HOP-1, after the founding member of the meiotic HORMA
222 proteins, *S. cerevisiae* Hop1. We raised a polyclonal antibody by genetic immunization using a
223 fragment that encodes a peptide of 100 amino acids in length, including part of the HORMA
224 domain, and found that this antibody indeed recognized chromosome axes from meiotic entry
225 through late prophase.

226 To enable cytological detection of synaptonemal complex (SC) assembly, we searched
227 for homologs of SC proteins. This is notoriously challenging due to rapid divergence of these
228 proteins, and their extensive regions of coiled-coil potential, which is associated with a strongly
229 skewed amino acid composition. *C. elegans* expresses four known SC proteins, known as SYP-
230 1, SYP-2, SYP-3, and SYP-4 (Colaiácovo et al., 2003; MacQueen et al., 2002; Smolikov et al.,
231 2009, 2007). SYP-4 contains a distinctive C-terminal domain with several unusual motifs
232 enriched in glycine and phenylalanine residues. We generated and sequenced an RNA library

233 from isolated gonads, which facilitated identification of full-length *Ppa-syp-4*. We inserted an
234 HA epitope tag at the C-terminus of the protein via template-directed repair of a CRISPR/Cas9-
235 induced break, and found that immunofluorescence with an epitope-specific antibody
236 localized specifically between paired meiotic chromosomes, confirming SYP-4::HA as a marker
237 for the SC (Figure 3A, B). The tagged protein supported normal meiosis, as indicated by the
238 low percentage of inviable embryos and males in the strain population (Figure 3 – Supplement
239 1).

240 HOP-1 was detected in the nucleoplasm in the premeiotic region of the germline and
241 formed linear structures along chromosomes upon meiotic entry. SYP-4 was detected along
242 chromosome segments shortly thereafter, and fully colocalized with HOP-1 tracks during
243 pachytene. Notably, the region of the germline containing nuclei with fully aligned stretches of
244 SYP-4 and HOP-1 was very short compared to *C. elegans*, in which SC disassembly occurs close
245 to the bend of the gonad arm, shortly prior to diakinesis. In contrast, SC disassembly initiated
246 much earlier in *P. pacificus*; the major fraction of prophase nuclei is best described as “pachy-
247 diplotene,” since chromosomes remain only partially synapsed. Six short stretches of SYP-4
248 were apparent in these nuclei, which persisted over an extended region (Figure 3A, B). This
249 asymmetrical pattern of the SC is highly reminiscent of a more transient stage in *C. elegans*, in
250 which the SC remains associated with the “short arm” of each homolog pair and subsequently
251 contributes to the step-wise loss of cohesion during the first and second meiotic divisions (Lui
252 and Colaiácovo, 2012; Zhang et al. 2018).

253 HOP-1 localized normally to chromosome axes in *spo-11* and *dmc-1* mutants, but
254 extensive SC assembly failed. Instead, small, dispersed puncta of SYP-4 were observed along

255 chromosome axes, with occasional longer tracks (Figure 3C). In contrast to *spo-11* and *dmc-1*
256 mutants, *rad-51* mutants displayed robust synapsis with a distribution of stages similar to that
257 seen in wild-type hermaphrodites (Figure 3C). These observations indicate that *spo-11* and
258 *dmc-1* play crucial roles during homologous synapsis in *P. pacificus*, while *rad-51* is dispensable
259 for this process. This further suggests that synapsis initiation may be tightly coupled to
260 homolog pairing and that SPO-11 and DMC-1, but not RAD-51, play central roles in this
261 process.

262

263 **DMC-1 and RAD-51 localize sequentially during distinct stages of meiotic prophase**

264 To investigate the functions of and interplay between DMC-1 and RAD-51 in *P.*
265 *pacificus*, we inserted a V5 epitope tag at the C-terminus of DMC-1 using CRISPR/Cas9, and
266 raised a polyclonal antibody that recognizes Ppa-RAD-51 (see Materials and Methods). DMC-
267 1::V5 supported normal meiosis, as evidenced by a normal brood size, high embryonic viability
268 and low percentage of males (Figure 3 – Supplement 1). Surprisingly, the two proteins showed
269 distinct and nonoverlapping patterns of localization. DMC-1 localized broadly, appearing to
270 coat the chromosomes, in transition zone nuclei and disappeared immediately upon
271 completion of synapsis. RAD-51 displayed a much more restricted, punctate distribution along
272 chromosomes, and was only detected in nuclei in which DMC-1 no longer coated the
273 chromosomes (Figure 4A, B). Occasional nuclei at the border between the transition zone and
274 pachytene region exhibited both DMC-1 and RAD-51, although DMC-1 was very faint in these
275 nuclei and did not overlap with RAD-51 (Figure 4C). Additionally, DMC-1 remained strongly
276 associated with chromosomes in some late nuclei that retained clustered DAPI morphology,

277 presumably either “straggler” nuclei with delays in synapsis or CO designation, or apoptotic
278 cells, both of which are typically observed in the germlines of wild-type *C. elegans* (Figure 4D).

279 We also tested the interdependence of DMC-1 and RAD-51 recombinases for their
280 localization. In *S. cerevisiae* and *A. thaliana*, Dmc1 functions as an essential catalyst for
281 interhomolog joint molecule formation during meiotic DSB repair, while Rad51 acts as an
282 accessory protein for Dmc1 nucleofilament formation (Cloud et al., 2012; Da Ines et al., 2013).
283 We did not detect RAD-51 along chromosomes in the transition zone, where DMC-1 was
284 abundant on chromatin, and we found that DMC-1::V5 localization was normal in *rad-51*
285 mutants, indicating that RAD-51 does not play an essential role in the recruitment of DMC-1
286 (Figure 4 – Supplement 1A). Conversely, RAD-51 was also observed in some nuclei in *dmc-1*
287 mutants, specifically in late prophase nuclei proximal to the extended transition zone (Figure 4
288 – Supplement 1B). RAD-51 foci were both more abundant and larger in *dmc-1* mutants
289 compared to wild-type pachytene nuclei, perhaps due to persistent unrepaired DSBs that
290 accumulate in the absence of DMC-1 protein. Alternatively, the bright foci of RAD-51 observed
291 in late prophase nuclei could be indicative of an apoptotic response to unrepaired breaks
292 and/or extensive asynapsis.

293 In *spo-11* mutants, which are expected to lack any meiotic DSBs, DMC-1 failed to
294 localize to chromosomes, and instead formed nuclear aggregates (Figure 4 – Supplement 1C).
295 It was unclear whether these DMC-1 aggregates were associated with chromatin. Since DMC-1
296 localizes broadly to chromosomes during early prophase, rather than specifically at
297 recombination intermediates, this suggests that the mislocalization reflects *spo-11*-dependent

298 regulation of DMC-1, likely through activation of a DNA damage signaling pathway, rather
299 than an absence of potential binding sites.

300 In contrast to DMC-1, RAD-51 does appear to associate specifically with recombination
301 intermediates. Thus, it was unsurprising to see that RAD-51 foci were absent from meiotic
302 nuclei in *spo-11* mutants (Figure 4 – Supplement 1E). Some RAD-51 foci were observed in the
303 premeiotic region of *spo-11* mutants, as in wild-type animals, providing a positive control for
304 immunofluorescence (Figure 4 – Supplement 1D).

305 Together these observations indicate that DMC-1 and RAD-51 bind to chromatin at
306 different stages of meiotic prophase and are not interdependent, although both require DSBs
307 for their chromosome localization.

308

309 **RAD-51 is not required for CO formation or completion of meiosis**

310 To assess the roles of DMC-1 and RAD-51 in CO formation, we quantified the number of
311 DAPI-staining bodies at diakinesis in *dmc-1* and *rad-51* mutants. Wild-type oocytes at this
312 stage contained ~6 DAPI-staining bodies (average= 5.6), as expected, while in *spo-11* mutants,
313 ~12 DAPI-staining bodies were present (average= 11.5), consistent with a complete failure of
314 CO formation in the absence of DSBs (Figure 5A,B). Interestingly, in *dmc-1* mutant germlines
315 we frequently failed to detect oocytes at diakinesis, indicative of a defect in meiotic
316 progression and the likely activation of a checkpoint in response to unrepaired DSBs. In cases
317 when we did observe nuclei at diakinesis, they contained an average of 11.6 DAPI-staining
318 bodies, reflecting a complete absence of COs, as in *spo-11* mutants (Figure 5C, D).

319 Somewhat surprisingly, disruption of *rad-51* resulted in homozygous mutant
320 hermaphrodites that were viable and fertile, although animals produced smaller broods and
321 their embryos showed greatly reduced viability (Figure 5E). Homozygous *rad-51* mutant
322 gonads also displayed diakinesis nuclei more frequently than *dmc-1* mutants, although they
323 were absent in 2 out of 20 gonads scored, indicating that loss of DMC-1 function impairs
324 meiotic progression more severely than loss of RAD-51 (Figure 5C, D). Consistent with this
325 observation, while *rad-51* mutants had a lower average brood size compared to wild-type
326 animals, *dmc-1* mutants had even smaller broods, ranging from zero to 35 embryos laid per
327 mutant homozygote (Figure 5E). In striking contrast to *Cel-rad-51* mutants, which display
328 fragmented chromatin aggregates at diakinesis (Martin et al., 2005; Rinaldo et al., 2002), *Ppa-*
329 *rad-51* mutants displayed an average of 6 DAPI-staining bodies, similar to wild-type (Figure
330 5B). Together with the relatively high viability of progeny of *rad-51* homozygous mutants, this
331 indicates that RAD-51 does not play an essential role in CO formation in *P. pacificus*.

332

333 **Conserved CO factor COSA-1 marks Class I COs in *P. pacificus***

334 To further analyze CO formation in *P. pacificus*, we identified the gene encoding the
335 metazoan meiotic cyclin-related protein COSA-1/Cntd1 and inserted a 3xFLAG epitope tag at
336 the C-terminus of the coding sequence via CRISPR/Cas9. The strain expressing COSA-
337 1::3xFLAG yielded progeny with high embryonic viability and low percentage of males,
338 demonstrating that the tagged protein functions sufficiently to support normal meiosis (Figure
339 3 – Supplement 1). Immunostaining with anti-FLAG antibodies revealed discrete foci along the
340 SC, beginning as early as zygotene, which decreased in number and became more intense

341 during the brief pachytene region (Figure 6A, B). Most pachytene nuclei displayed 6 COSA-1
342 foci, each of which was associated with an individual SC between each pair of homologous
343 chromosomes (Figure 6C and Supplemental Video 1). Previous genetic mapping experiments
344 revealed that homolog pairs often experience multiple COs in *P. pacificus* (Srinivasan et al.,
345 2002). To investigate whether these extra COs might arise specifically during
346 spermatogenesis, we analyzed younger J₄ hermaphrodites, which had not yet undergone the
347 switch from spermatogenesis to oogenesis, and found that pachytene nuclei undergoing
348 spermatogenesis also displayed ~6 COSA-1 foci (Figure 6- figure supplement 1). This suggests
349 that *P. pacificus*, like *C. elegans*, exhibits complete chromosome-wide Class I CO interference
350 and, combined with previous genetic data, implies that additional COs likely arise through the
351 Class II CO pathway, which does not require COSA-1.

352 Intriguingly, SC disassembly appeared to be regulated by the position of the lone Class I
353 CO between each chromosome pair, as in *C. elegans*. By mid-pachy-diplotene, 6 short
354 stretches of SYP-4::HA were observed, each associated with a single COSA-1::3xFLAG focus
355 near one end (Figure 6B). During late prophase, COSA-1::3xFLAG foci were no longer visible,
356 although short stretches of SYP-4::HA could still be observed. We observed splaying of
357 chromosome axes along the long arms upon removal of the central region proteins (Figure
358 6D). HOP-1 was retained on both arms upon disassembly of the SC, although the signal
359 appeared fainter along the long arms, perhaps due to splitting of the signal. At this stage, short
360 stretches of SYP-4::HA colocalize with corresponding bright stretches of HOP-1 (Figure 3B and
361 Figure 6D). Bivalents at diakinesis also show a cruciform structure similar to that seen in *C.*
362 *elegans*, indicative that only the Class I COs give rise to chiasmata that persist until diakinesis.

363 We next examined the localization of COSA-1::3xFLAG in various mutant backgrounds.
364 As expected, *dmc-1* mutants showed a complete absence of COSA-1 foci throughout prophase,
365 while 6 foci were readily observed in pachytene nuclei in *rad-51* mutants (Figure 7A). These
366 observations were consistent with the number of DAPI-staining bodies we observed at
367 diakinesis (Figure 5B). Surprisingly, a few bright COSA-1::3xFLAG foci were present throughout
368 prophase in *spo-11* mutants (Figure 7A). However, since ~12 DAPI-staining bodies were
369 observed during diakinesis, we conclude that these COSA-1 foci do not mark designated COs.
370 A similar phenomenon has been reported in *C. elegans spo-11* mutants (Nadarajan et al., 2017;
371 Pattabiraman et al., 2017), suggesting that COSA-1 can coalesce at sites lacking bona fide
372 recombination intermediates.

373

374 DISCUSSION

375

376 Distinct roles of Dmc1 and Rad51

377 Rad51 and Dmc1 show very similar activities *in vitro*; both are capable of binding to
378 single-stranded and double-stranded DNA *in vitro*, although both show a strong preference for
379 ssDNA binding (Hong et al., 2001; Li et al., 1997; Masson et al., 1999). However, these proteins
380 clearly play non-redundant functions in meiosis. This is thought to be due in part to the activity
381 of Dmc-1 specific cofactors Mnd1 and Hop2, as well as differential regulation of the timing and
382 activities of the two paralogs. Our analysis of the two RecA homologs in *P. pacificus*, RAD-51
383 and DMC-1, defines their distinct contributions during meiosis.

384 DMC-1 appears to coat much of the chromatin in transition zone nuclei, whereas RAD-
385 51 shows a much more punctate localization, and only after DMC-1 is largely removed from
386 chromosomes. These observations suggest that DMC-1 interacts extensively with double-
387 stranded DNA, while RAD-51 localizes specifically to single-stranded DNA at sites of active
388 recombination. Intriguingly, even though DMC-1 apparently localizes much more broadly, both
389 DMC-1 and RAD-51 depend on SPO-11 for their association with meiotic chromosomes. We
390 interpret these observations to indicate that the binding of DMC-1 to chromatin is regulated by
391 a mechanism that responds to SPO-11 activity, likely through activation of a DNA damage
392 response pathway. In contrast, the association of RAD-51 with recombination intermediates is
393 likely inhibited by this pathway, and is only permitted after DMC-1 has ensured the formation
394 of CO intermediates between each pair of chromosomes.

395 The sequential localization of DMC-1 and RAD-51 first suggested that they function
396 independently, and this is supported by our analysis of loss-of-function mutations. By contrast
397 to budding yeast and *A. thaliana*, RAD-51 is dispensable for the activity of DMC-1 in pairing,
398 synapsis, and CO formation. Instead, RAD-51 appears to play a supporting role in DSB repair
399 during pachytene, processing excess DSBs that remain after CO designation has occurred. In *C.*
400 *elegans*, which expresses only RAD-51, a similar switch between two modes of double-strand
401 break repair is nevertheless observed during meiotic prophase (Hayashi et al., 2007).
402 Association of Ce-RAD-51 with repair intermediates is differentially regulated from the onset
403 of meiosis until a mid-pachytene transition that coincides with CO designation; at this time,
404 competence to convert DSBs to interhomolog COs is also lost. Recent work revealed an
405 analogous switch from a “meiotic” repair to a “somatic”-like repair pathway during the

406 transition from mid- to late pachytene in mouse spermatocytes (Enguita-Marruedo et al.,
407 2019). In *P. pacificus*, it is thus likely that DMC-1 and RAD-51 have highly specialized functions:
408 formation of interhomolog COs by DMC-1 in the transition zone and a more general mode of
409 double-strand break repair by RAD-51 during pachytene. Furthermore, our observation that
410 nuclei in *rad-51* mutants display cruciform bivalents and lack fragmented chromatin at
411 diakinesis suggests that excess DSBs can be repaired through an alternate pathway which does
412 not depend on RAD-51 activity, such as non-homologous end joining, or that DMC-1 can
413 compensate for RAD-51 but not the other way around. The nature of RAD-51-dependent DSB
414 repair and how the activities of RAD-51 and DMC-1 are regulated in early meiotic prophase will
415 be a focus of future investigation in this species.

416

417 **CO regulation in *P. pacificus***

418 Genetic mapping in *P. pacificus* revealed lengths of ~100-250 centimorgans for each
419 chromosome, corresponding to 2-5 interhomolog COs per meiosis (Srinivasan et al., 2003,
420 2002). By contrast, the genetic map of each chromosome in *C. elegans* is 50 cM, reflecting a
421 single CO per pair (Hillers et al., 2017). Surprisingly, our analysis of Ppa-COSA-1 localization
422 revealed only a single COSA-1 focus per chromosome by pachytene, very similar to what is
423 seen in *C. elegans* (Yokoo et al., 2012). This suggests that either multiple Class I COs occur but
424 only one retains COSA-1, or that all but a single CO forms by an alternate, COSA-1-
425 independent pathway. In many eukaryotic systems, two CO pathways co-exist (Gray and
426 Cohen, 2016). Class I COs show spatial interference and depend on factors including MSH-4/5,
427 ZHP-3/Rnf212, and COSA-1/Cntd1. On the other hand, Class II COs do not exhibit interference

428 and undergo an alternate resolution pathway that requires the structure-specific endonuclease
429 complex Mus81-Eme1/Mms4. In some species, notably in *A. thaliana* and *S. cerevisiae*, Class II
430 COs can occur in the absence of Class I COs, but this may not be the case in all organisms.
431 Future work will examine whether all COs in *P. pacificus* arise only after the single, obligate
432 Class I CO has been designated, and whether the designation of Class I COs is necessary for the
433 formation and resolution of Class II COs. We further note that there appears to be only one
434 chiasma formed between each homolog pair, which is likely created by the lone COSA-1-
435 associated Class I CO. Our work reveals the potential of *P. pacificus* to address some long-
436 standing questions about mechanisms and regulation of CO recombination that are not
437 accessible in the meiotic model *C. elegans* due to the absence of Class II COs during normal
438 meiosis.

439

440 **Comparative analysis of meiosis reveals major variations within the nematode lineage**

441 In addition to establishing key aspects of meiosis in *P. pacificus*, this work also
442 illuminates the evolutionary history of meiosis in *C. elegans*. A body of prior work has revealed
443 that recombination-independent homologous synapsis in *C. elegans* relies on pairing centers,
444 specialized chromosome regions that interact with nuclear envelope and drive chromosome
445 movement during early prophase. These meiosis-specific dynamics are typically mediated by
446 telomeres, but have shifted to a unique region on each chromosome in *C. elegans*. Pairing
447 centers also act as the sites of synapsis initiation (Rog and Dernburg, 2013). By contrast, in
448 other organisms, telomere-led chromosome movement is thought to promote homologous
449 interactions, but stabilization of pairing and initiation of synapsis occur at early recombination

450 intermediates, which depend on Spo11 and Dmc1 activity. Pairing center activity depends on
451 and is largely defined by the recruitment of a family of zinc finger proteins that bind to DNA
452 sequence motifs in these regions (Phillips et al., 2009). These proteins, known as ZIM-1, ZIM-2,
453 and ZIM-3, and HIM-8 in *C. elegans*, also act as scaffolds to recruit a cascade of kinase activities
454 required for pairing and synapsis (Harper et al., 2011; Kim et al., 2015; Labella et al., 2011).
455 Surprisingly, most of the sequenced genomes of nematodes in Clade V include both homologs
456 of the HIM-8/ZIM family and orthologs of Dmc1, Hop2, and Mnd1 (Figure 2 – Supplement 1).
457 The *Pristionchus* genus is unusual within this Clade in that it lacks apparent homologs of the
458 pairing center proteins, while *Caenorhabditids* are among the few genera that have lost
459 Dmc1/Mnd1/Hop2, which were independently lost along the branch leading to *Oscheius tiuplae*
460 and *Auanema rhodensis*. This suggests that the dominant role of pairing centers in homologous
461 synapsis is likely to be recently derived, perhaps restricted to *Caenorhabditids*. Future studies
462 of species in which Dmc1 and pairing center proteins co-exist may illuminate how synapsis
463 initiation activity relocated from sites of Dmc1-mediated strand exchange to pairing centers.
464 In addition to clarifying how pairing centers acquired their central meiotic roles in *C. elegans*,
465 further analysis may help to address the longstanding question of how recombination
466 intermediates trigger initiation of synapsis.

467 *C. elegans* is a popular and powerful model system for molecular studies of meiosis. *P.*
468 *pacificus* shares many of the same experimental advantages, although naturally has fewer
469 experimental tools, since it has been developed far more recently. Genome engineering using
470 CRISPR/Cas9 is somewhat more challenging, and has so far been refractory to large insertions,
471 such as fluorescent proteins. However, this barrier will likely be overcome through advances in

472 editing efficiency. Perhaps a greater obstacle is the absence of balancer chromosomes, which
473 are invaluable for maintaining mutations that reduce viability or fertility in *C. elegans*. Because
474 balancers are unavailable for *P. pacificus*, most of the mutations described in this work have
475 been maintained in unbalanced heterozygotes through frequent, labor-intensive genotyping
476 assays. Moreover, the analysis presented here suggests that it may not be possible to construct
477 crossover-suppressing balancer chromosomes, given that recombination is essential for
478 homolog pairing and synapsis. By contrast, the derived, recombination-independent
479 mechanism of pairing and synapsis in *C. elegans* makes it possible to propagate large-scale
480 chromosome rearrangements that suppress meiotic recombination over large genomic regions
481 while maintaining regular segregation of chromosomes.

482 The advent of broadly applicable techniques for genome editing has enabled rapid
483 progress towards developing *P. pacificus* for molecular studies, along with many other
484 experimental models. Future exploration of meiosis in *P. pacificus*, and perhaps in other
485 nematode models, will further expand our understanding of core mechanisms and plasticity of
486 sexual reproduction.

487

488 **MATERIALS AND METHODS**

489 *P. pacificus* strains and maintenance

490 Animals were cultured on NGM media with *E. coli* OP50 at 20°C under the same
491 standard conditions as *C. elegans* (Brenner, 1974). The wild-type strain is a derivative of PS312
492 designated as “g7,” which was provided by Ralf Sommer. This isolate was found to be more
493 amenable to genome editing by CRISPR-Cas9 than the parental strain. Mutant alleles were

494 maintained in a heterozygous state. Every few generations and before each
495 immunofluorescence or FISH experiment, single adult hermaphrodites were picked to new
496 plates and allowed to lay embryos for two days, after which the genotype of the parent was
497 determined by PCR genotyping. Progeny from heterozygous mothers, one-fourth of which are
498 homozygous for the meiotic mutation, were analyzed using the assays described here;
499 heterozygous and wild-type siblings were frequently used as controls, in addition to analysis of
500 unedited wild-type animals.

501

502 *CRISPR/Cas9 genome editing*

503 To modify the *P. pacificus* genome, we adapted our preferred CRISPR/Cas9 protocol
504 from *C. elegans* to *P. pacificus*. Equimolar quantities of Alt-R[®] CRISPR-Cas9 crRNA and
505 tracrRNA molecules (Integrated DNA Technologies, Coralville, IA) were hybridized using a
506 thermocycler (95°C for 5 minutes, then 25°C for 5 minutes). 4µl of 100µM hybridized
507 tracrRNA/crRNA was combined with 4µl of 40µM *S. pyogenes* Cas9-NLS purified protein (QB3
508 Macrolab, UC Berkeley, Berkeley, CA) and incubated at room temperature for 5 minutes. 2µl of
509 100µM stock of an Ultramer[®] DNA oligo (IDT) repair template containing 50-60 bp homology
510 arms and the desired epitope or mutation sequence was added to the mixture, for a total
511 volume of 10µl, and injected into the gonads of 24 hour-post J4 adult hermaphrodites.
512 Following a 2-4 hour recovery period, injected animals were allowed to lay embryos at 20°C for
513 16-20hr. Four days later, a fraction of the F1 population (typically 150-200 progeny from 6-8
514 injected P₀s) was screened for the presence of the mutation or epitope tag sequence by PCR
515 genotyping, and candidate alleles were verified by Sanger sequencing. A complete list of

516 crRNA, repair template, and genotyping primer sequences used to generate alleles in this
517 study is provided as Table S1.

518 TALEN constructs were generated using a protocol adapted from Zhang et al. (2011)
519 and designed using the TAL Effector Nucleotide Targeter 2.0 website ([https://tale-
520 nt.cac.cornell.edu/](https://tale-
520 nt.cac.cornell.edu/)).

521

522 *Viability and fertility*

523 To quantify embryonic viability, brood size, and male progeny of wild-type and *rad-51*
524 mutants, J₄ hermaphrodites were picked onto individual plates and transferred every 24 hours
525 over 72 hours total. Embryos were counted each day, after transferring the adult
526 hermaphrodite to a new plate, and kept at 20°C. Three to four days later, adults were counted
527 on each plate. To analyze *spo-11* and *dmc-1* mutants, 24 individual J₄ hermaphrodites were
528 picked from progeny of a verified heterozygous mutant hermaphrodite. Quantification was
529 performed as in wild type, but after 72 hours, the adult hermaphrodite was lysed and
530 genotyped for the presence of the mutation. Thus, although 24 animals total were quantified
531 from a mixed population of *spo-11*/+ or *dmc-1*/+ animals, data from 5 homozygous *spo-11* and 7
532 homozygous *dmc-1* mutant animals are reported in the data table, Figure 5E.

533

534 *Immunofluorescence and FISH*

535 To stage animals for each experiment, 30-40 J₄s were picked from a PCR-verified
536 heterozygous mother onto a fresh plate and allowed to develop for an additional 24 or 48
537 hours at 20°C. Young adult hermaphrodites were dissected on a clean coverslip in egg buffer

538 containing 0.05% tetramisole and 0.1% Tween-20. Samples were fixed for 2 minutes in egg
539 buffer with 1% formaldehyde and transferred to a 1.5-ml tube containing PBST. After 5
540 minutes, the PBST was replaced with ice-cold methanol and incubated at room temperature
541 for an additional 5 minutes. Worms were washed twice with PBST, blocked with Roche
542 blocking reagent, and stained with primary antibodies diluted in Roche blocking solution for
543 1.5-2 hours at room temperature. Samples were washed with PBST and incubated with
544 secondary antibodies raised in donkey and conjugated with Alexa-488, Cy3 or Cy5 (Jackson
545 ImmunoResearch Laboratories, West Grove, PA). Worms were then incubated with 1µg/ml
546 DAPI in PBST, washed with PBST, and mounted in ProLong™ Gold antifade mounting solution
547 (Invitrogen) before imaging.

548 For embryo staining, 20 plates of mixed-stage worms were harvested with water and
549 treated with 1:8 solution of bleach:water for 5 minutes at room temperature. Embryos were
550 collected by centrifugation and washed twice with PBS. To dissolve the vitelline membrane, a
551 solution containing 2.6 ml of n-heptane, 2 ml of PBS, and 1% paraformaldehyde (final) was
552 added to the embryo pellet for 5 minutes at room temperature with shaking. Treated embryos
553 were collected by centrifugation, washed twice with 5 ml MeOH, three times with PBS, and
554 incubated with Roche blocking reagent, primary, and secondary antibodies as described
555 above. Embryos were mounted on agarose pads for imaging.

556 For FISH experiments, age-matched animals were dissected and fixed as for
557 immunofluorescence experiments described above, except that the initial fixation was for 4
558 minutes in 2% formaldehyde. After incubation in ice-cold methanol, worms were washed with
559 2x SSCT twice and incubated in 50% 2x SSCT/50% formamide solution overnight at 37°C. The

560 next day, the worms were transferred to a small PCR tube, excess solution was removed from
561 the sample, and a 40 µl hybridization mix containing 250ng of each probe in hybridization
562 buffer (3.5xSSC, 58% formamide, 12.75% dextran sulfate) was added. The sample was
563 immediately denatured in a thermocycler at 91°C for 2 minutes and incubated overnight at
564 37°C. On the last day, the worms were transferred to a 1.5-ml tube and washed with 2xSSCT.
565 After 5 minutes, the solution was replaced with fresh 2xSSCT and mounted with ProLong™
566 Diamond Antifade Mountant with DAPI (Invitrogen).

567

568 *FISH probes*

569 Probes for a central locus on chromosome IV and the left end of chromosome X were
570 designed based on two short tandem repeat motifs. Tandem Repeat Finder v4.09 (Benson,
571 1999) was used to identify tandem repeats in *P. pacificus* "El Paco" genome assembly
572 (Rödelsperger et al., 2017) using default parameters and a maximum periodicity of 200 bp. The
573 output was then filtered to identify repeats that spanned more than 8 kb. These were
574 compared to the genome sequence using BLAST to identify the subset of sequences restricted
575 to a single major locus per genome. A subset of these repeats was then tested for specific and
576 robust hybridization with oligonucleotide probes. The Chromosome IV probe targets the 30-
577 base repeated motif TCATTGAAATGATCACAATCATTGA, which spans 40.1 kb at a position
578 11.3 Mb from the left end of chromosome IV. The Chromosome X probe
579 (GGTGGTCGACGGCTGCGTCG) targets a 30-base repeat motif that spans two very close
580 regions of 29.3kb and 11.1kb on the left end of the X chromosome. Single-stranded

581 oligonucleotides labeled at the 3' end with 6-FAM or Cy3 dyes were purchased from IDT and
582 used directly as FISH probes.

583

584 *Antibodies*

585 Antibodies against Ppa-RAD-51 were generated against a 6x His-tagged N-terminal
586 fusion protein (aa 1-103) expressed and purified from bacteria. Four mice were immunized with
587 the antigen. Serum from one animal, designated S148, was used without purification at 1:300
588 dilution (Pocono Rabbit Farm and Laboratory, Canadensis, PA). Antibodies against Ppa-HOP-1
589 were generated by genetic immunization against aa 177-276 (SDIX, Newark, DE) and used in
590 the following experiments at 1:300 dilution. Additional antibodies were purchased from
591 commercial sources and diluted as follows: mouse anti-FLAG (1:500, Sigma #F1804), mouse
592 anti-V5 (1:500, Thermo Fisher #R960-25), rabbit anti-V5 (1:250, Millipore Sigma #V8137), and
593 goat anti-HA (1:500, Novus Biologicals #NB600-362). Secondary antibodies raised in donkey
594 and labeled with Alexa 488, Cy3, or Cy5 were used at 1:400 dilution (Jackson ImmunoResearch
595 Laboratories).

596

597 *Orthology analysis and phylogenetic inference*

598 Accessions to all data used in orthology analysis are available in Table S2. We
599 downloaded the predicted protein sequences of 65 nematode species and five outgroup taxa
600 and filtered for the longest isoform of each gene. OrthoFinder (Emms and Kelly, 2015) was
601 used to cluster all protein sequences into putative orthologous groups (OGs) using the default
602 inflation value of 1.5. OGs containing loci which were present in at least 75% of species and

603 which were, on average, single copy (mean < 1.3) were selected. We aligned each selected OG
604 using MAFFT (Kato and Standley, 2013) and generated a maximum likelihood tree along with
605 1000 ultrafast bootstraps (Hoang et al., 2018) using IQ-TREE (Nguyen et al., 2015), allowing the
606 best-fitting substitution model to be selected automatically (Kalyaanamoorthy et al., 2017).
607 Each tree was screened by PhyloTreePruner (Kocot et al., 2013); collapsing nodes with
608 bootstrap support <90), and any OGs containing paralogues were discarded. If two
609 representative sequences were present for any species (*i.e.*, “in-paralogs”) after this paralog
610 screening step, the longest of the two sequences was retained and the other discarded. We
611 then realigned the remaining OGs using MAFFT and trimmed spuriously aligned regions using
612 trimAl (Capella-Gutiérrez et al., 2009). The trimmed alignments were subsequently
613 concatenated using catfasta2phyml (available at <https://github.com/nylander/catfasta2phyml>)
614 to form a supermatrix. We inferred the nematode species tree using IQ-TREE with the general
615 time reversible model (GTR) with gamma-distributed rate variation among sites. The resulting
616 tree was visualized using iTOL (Letunic and Bork, 2016).

617 We identified the OGs which contain orthologs of DMC-1, MND-1, HOP-2 and RAD-51
618 using BLASTP to search using the orthologous protein sequences from *Homo sapiens* as
619 queries. The OG containing the *C. elegans* proteins HIM-8, ZIM-1, ZIM-2, ZIM-3 was identified
620 using the appropriate transcript IDs. Each OG was aligned using MAFFT and a gene tree was
621 inferred using IQ-TREE, allowing the best-fitting substitution model to be selected
622 automatically. Each gene tree was visually inspected using iTOL.

623

624 *Total RNAseq*

625 Total RNA was isolated from 20 whole worms or 30 dissected gonads from 48 h post J4
626 animals using TRIzol (Invitrogen). TruSeq Stranded Total RNA (Illumina) sequencing libraries
627 were constructed following the manufacturer's instructions. For both conditions, three
628 independent libraries were constructed. Libraries were pooled and sequenced on a HiSeq4000
629 (150bp, PE, QB3 Vincent J. Coates Genomics Sequencing Laboratory). Reads were mapped to
630 the "El Paco" genome assembly including annotated splice sites (Rödelsperger et al., 2017)
631 using STAR. To correct misannotated splice sites, a transcriptome was then reconstructed de
632 novo using StringTie. Transdecoder was used to generate potential open reading frames. To
633 identify potential meiotic genes, we identified genes enriched in dissected gonads over whole
634 worms using HTSeq and edgeR.

635

636 **Acknowledgements**

637 This work was supported by funding from the Howard Hughes Medical Institute to AFD
638 and a fellowship from the Helen Hay Whitney Foundation to JB. This work used the Vincent J.
639 Coates Genomics Sequencing Laboratory at UC Berkeley, supported by NIH S10 OD018174
640 Instrumentation Grant. We are grateful to Ralf J. Sommer, Ray Hong, and other members of
641 the *P. pacificus* research community for providing us with *P. pacificus* strains and abundant
642 helpful advice. We thank members of the Dernburg lab for helpful discussions about this work
643 and critical reading of the manuscript.

644

645 **Figure Legends**

646 **Figure 1.** Germline organization and meiotic progression in *P. pacificus* is superficially similar to
647 *C. elegans*. A. Projection image of a *P. pacificus* hermaphrodite gonad stained with DAPI. Scale
648 bar, 30 μm . Insets show representative nuclei from the premeiotic region (PM), transition zone
649 (TZ), pachytene (Pach), diplotene (Dip), diffuse stage (Diff) and diakinesis. Scale bar, 5 μm . B.
650 Distal region of a *P. pacificus* germline injected with 0.3 nM Cy3-dUTP solution, dissected and
651 stained with DAPI after 30 minutes of recovery. Scale bar, 30 μm . C. Mitotic chromosomes
652 (DAPI) in a 2-4 cell stage embryo and the premeiotic germline of adult hermaphrodites
653 expressing CENP-C::V5 (magenta). Scale bar, 2 μm .

654
655 **Figure 2.** Stable homolog pairing requires early recombination factors. A. Diagram showing
656 the locations of tandem repeat sequences used to generate DNA FISH probes for pairing
657 analysis in *P. pacificus*. B. Representative images show the progression of homolog pairing of
658 Chromosome X (magenta) and Chromosome IV (yellow) during meiotic prophase in wild-type
659 hermaphrodites. Premeiotic region (PM), transition zone (TZ), and pachytene (Pach). Scale
660 bar, 5 μm . C. Representative images of FISH probe signals in *spo-11*, *dmc-1*, and *rad-51* mutants
661 during mid-prophase stage (roughly equivalent to the pachytene stage in wild-type germlines).
662 Scale bar, 5 μm . D. Temporal progression of X and IV chromosome pairing in WT, *spo-11*, *dmc-*
663 *1*, and *rad-51* mutants. Distance between pairs of corresponding FISH signals were measured in
664 3D using Softworx or Prism for three gonads of each genotype. Each gonad was divided into
665 five zones of equal length, from the distal tip to the bend of the gonad arm, and the distances
666 between pairs of homologous FISH signals are presented in a scatter plot diagram. E. Distance
667 between pairs of heterologous FISH signals were measured in premeiotic (PM) and transition

668 zone (TZ) nuclei in WT, *spo-11* and *dmc-1* mutants (spanning zones 1 and 2 only). Distances
669 between pairs of homologous FISH signals (Chrom X and IV combined) in TZ nuclei are
670 included for comparison. *** $p < .0001$, by Student's *t*-test.

671
672 **Figure 2- figure supplement 1.** Partial representation of the nematode lineage, including 65
673 nematode species, and five outgroup taxa showing the presence of meiotic proteins. D= Dmc1;
674 M= Mnd1; H= Hop2; Z= HIM-8/ZIM-1,2,3. *C. elegans* and *P. pacificus* are highlighted in blue.

675
676 **Figure 2- figure supplement 2.** A. Composite projection images of whole gonads stained with
677 DAPI from WT, *spo-11*, *dmc-1*, and *rad-51* mutants. The extent of the transition zone of each
678 gonad is underlined with dashed lines. Scale bar, 30 μ m. B. Quantification of transition zone
679 length relative to the length from meiotic onset to the end of pachytene in WT (n=7), *spo-11*
680 (n=7), *dmc-1* (n=7), and *rad-51* (n=10). Error bars indicate mean \pm standard deviation. *spo-11* and
681 *dmc-1* mutants show significant differences from WT ($p < 0.0001$) but not *Ppa-rad-51* ($p = 0.8426$)
682 by ordinary one-way ANOVA.

683
684 **Figure 3.** SPO-11 and DMC-1 are required, while RAD-51 is dispensable, for homologous
685 synapsis in *P. pacificus*. A. Composite projection image of a wild-type strain expressing Ppa-
686 SYP-4::HA, stained with DAPI (gray), anti-HOP-1 (red), and anti-HA (green). Meiotic
687 progression is from left to right. Scale bar, 30 μ m. B. Higher magnification images of wild-type
688 nuclei in the premeiotic region (PM), transition zone (TZ), pachytene (Pach), and pachy-
689 diplotene (P-D) stages. C. Localization of Ppa-SYP-4::HA and Ppa-HOP-1 in WT, *spo-11*, *dmc-1*,

690 and *rad-51* mutants during early and mid-prophase (roughly equivalent to the TZ and Pach
691 regions in wild-type germlines, respectively). Synapsis fails in *spo-11* and *dmc-1* mutants but
692 forms normally in the *rad-51* background. Scale bar, 5 μm .

693
694 **Figure 3- figure supplement 1.** All epitope-tagged proteins used in this study support normal
695 meiosis. Epitope-tagged alleles were generated by in-frame insertion into the endogenous
696 gene loci using CRISPR/Cas9 (see Materials and Methods), and homozygosed by selfing of
697 successfully edited progeny. Fidelity of meiotic segregation in the resulting strains was
698 analyzed by counting the frequency of viable embryos and male progeny among whole broods
699 from self-fertilizing hermaphrodites, as indicated. Quantification of wild-type broods is also
700 reported in Figure 5E.

701
702 **Figure 4.** DMC-1 and RAD-51 localize sequentially to meiotic chromosomes. A. Composite
703 projection image of a wild-type gonad expressing DMC-1::V5, stained with DAPI (blue), anti-V5
704 (magenta), and anti-RAD-51 (yellow). Meiotic progression is from left to right. Scale bar, 30
705 μm . Inset shows the distinct localization of DMC-1 (magenta) and RAD-51 (yellow) in the
706 transition zone and pachytene regions, respectively. Scale bar, 5 μm . B. Higher magnification
707 images of nuclei in the transition zone and pachytene region. DMC-1 is present along
708 chromatin in the transition zone and disappears at pachytene. By contrast, RAD-51 localizes to
709 discrete foci starting at pachytene. Scale bar, 5 μm . C. Occasional nucleus on the border of the
710 transition zone and pachytene region display both DMC-1 and RAD-51. The signals do not
711 completely overlap. Scale bar, 2 μm . D. Nucleus with clustered DAPI morphology and strong

712 association of DMC-1 during later prophase. DMC-1 localizes to chromatin in “straggler” cells
713 that presumably have not completed synapsis or CO designation, or are undergoing apoptosis.
714 Scale bar, 2 μ m.

715

716 **Figure 4- figure supplement 1.** DMC-1 and RAD-51 do not depend on each other for their
717 localization to chromosomes, but both require DSBs. A. DMC-1 (magenta) is abundant on
718 chromosomes in transition zone nuclei of *rad-51* mutants. Anti-RAD-51 immunofluorescence
719 was used to identify homozygous mutants among the progeny of heterozygotes. B. RAD-51
720 foci are observed in late pachytene nuclei, proximal to the extended transition zone, of *dmc-1*
721 mutants. RAD-51 foci appear larger and more numerous than in wild-type pachytene nuclei. C.
722 DMC-1 forms nuclear aggregates in *spo-11* mutants and does not localize along chromosomes.
723 D and E. RAD-51 foci are detected in premeiotic nuclei of *spo-11* mutants but are absent during
724 meiotic prophase.

725

726 **Figure 5.** CO formation requires SPO-11 and DMC-1, but not RAD-51. A. Representative
727 images of DAPI-staining bodies at diakinesis for each indicated genotype. Scale bar, 5 μ m. B.
728 Quantification of DAPI-staining bodies in the -1 oocyte at diakinesis for each indicated
729 genotype (*n*= represents number of nuclei scored). C. Quantification of gonads which lacked
730 nuclei with DAPI-staining bodies at diakinesis stage. *n* is the number of germlines scored for
731 each genotype. D. Representative images of wild type, *dmc-1*, and *rad-51* mutant proximal
732 germlines. In wild-type germlines, diakinesis nuclei with fully condensed DAPI-staining bodies
733 are present distal to the spermatheca. However, nuclei with late prophase stage DAPI

734 morphology are frequently found adjacent to the spermatheca in *dmc-1* mutants and more
735 rarely in *rad-51* mutants. Meiotic progression is from left to right. Scale bar, 5 μ m. E.
736 Frequencies of viable embryos and male progeny of whole broods from wild type, *spo-11*, *dmc-*
737 *1* and *rad-51* mutant hermaphrodites.

738
739 **Figure 6.** COSA-1/Cntd1 accumulates at a single site per chromosome pair. A. Composite
740 projection image of a wild-type strain expressing three epitope-tagged proteins (COSA-
741 1::3xFLAG, DMC-1::V5, and SYP-4::HA), stained with anti-FLAG, anti-V5 and anti-HA
742 antibodies. Scale bar, 30 μ m. B. Higher magnification images of nuclei from the transition zone
743 (TZ), pachytene (pach), mid- and late pachy-diplotene (P-D). COSA-1::3xFLAG (green) foci are
744 detected in transition zone nuclei but do not colocalize with DMC-1::V5 (cyan). Foci peak in
745 brightness in pachytene nuclei and gradually become dimmer until they are no longer detected
746 during late pachy-diplotene. In early to mid- pachy-diplotene nuclei, six short stretches of SYP-
747 4::HA (magenta) are observed per nucleus, each associated with a single COSA-1::3xFLAG
748 focus. Scale bar, 5 μ m. C. Histogram showing the number of COSA-1::3xFLAG foci observed
749 per nucleus in the pachytene region. Analysis was restricted to 15 nuclei per gonad
750 immediately proximal to the transition zone and lacking DMC-1::V5 signal. Five individual
751 gonads were analyzed, for a total of 75 nuclei scored. D. Partial projection of a representative
752 nucleus in mid to late pachy-diplotene, stained with anti-HOP-1 (blue), anti-HA (marking the
753 SC, magenta), and anti-FLAG (marking COSA-1, green). A single COSA-1::3xFLAG focus is
754 observed at a junction (marked with a red arrowhead) between the "short arm," where SYP-
755 4::HA is retained, and splayed "long arms" lacking SC but positive for HOP-1. Scale bar, 2 μ m.

756

757 **Figure 6 - figure supplement 1.** COSA-1/Cntd1 accumulates at a single site per chromosome
758 pair during spermatogenesis. Composite projection image of a wild-type gonad from a J4-
759 stage hermaphrodite expressing COSA-1::3xFLAG (green) and SYP-4::HA (magenta). Scale
760 bar, 30 μm . At this stage the germline is still undergoing spermatogenesis. Inset shows a
761 higher magnification image of nuclei in the pachytene region. As during oogenesis, ~6 COSA-
762 1::3xFLAG foci are observed in pachytene nuclei during spermatogenesis. Scale bar, 5 μm .

763

764 **Figure 6 - Supplemental Video 1.** COSA-1/Cntd1 accumulates at a single site per chromosome
765 pair. 3D volume rendering of a single nucleus from the pachytene region of a wild-type worm
766 expressing COSA-1::3xFLAG (green) and SYP-4::HA (magenta). Each frame is a maximum
767 intensity projection from a region of a deconvolved 3D image. Each stretch of SYP-4::HA is
768 associated with a COSA-1::3xFLAG focus.

769

770 **Figure 7.** COSA-1::3xFLAG accumulates at sites of presumptive Class I COs. A. Nuclei from
771 hermaphrodites of the indicated genotype displaying COSA-1::3xFLAG (green) in early and
772 mid-prophase (roughly equivalent to the transition zone and pachytene regions in wild-type
773 germlines, respectively). COSA-1 foci are absent in *dmc-1* mutants, but 6 foci per nucleus are
774 detected in wild type and *rad-51* mutants. A few small foci are detected in *spo-11* mutants.
775 Scale bar, 5 μm .

776

777

778 REFERENCES

- 779 Aravind L, Koonin EV. 1998. The HORMA domain: a common structural denominator in mitotic
780 checkpoints, chromosome synapsis and DNA repair. *Trends Biochem Sci* **23**:284–286.
- 781 Benson G. 1999. Tandem repeats finder: a program to analyze DNA sequences. *Nucleic Acids*
782 *Research*. doi:10.1093/nar/27.2.573
- 783 Bishop DK, Park D, Xu L, Kleckner N. 1992. DMC1: A meiosis-specific yeast homolog of E. coli
784 recA required for recombination, synaptonemal complex formation, and cell cycle
785 progression. *Cell* **69**:439–456. doi:10.1016/0092-8674(92)90446-j
- 786 Bolt BJ, Rodgers FH, Shafie M, Kersey PJ, Berriman M, Howe KL. 2018. Using WormBase
787 ParaSite: An Integrated Platform for Exploring Helminth Genomic Data. *Methods Mol Biol*
788 **1757**:471–491. doi:10.1007/978-1-4939-7737-6_15
- 789 Brenner S. 1974. The genetics of *Caenorhabditis elegans*. *Genetics* **77**:71–94.
- 790 Capella-Gutiérrez S, Silla-Martínez JM, Gabaldón T. 2009. trimAl: a tool for automated
791 alignment trimming in large-scale phylogenetic analyses. *Bioinformatics* **25**:1972–1973.
792 doi:10.1093/bioinformatics/btp348
- 793 Christophorou N, Rubin T, Huynh J-R. 2013. Synaptonemal complex components promote
794 centromere pairing in pre-meiotic germ cells. *PLoS Genet* **9**:e1004012.
795 doi:10.1371/journal.pgen.1004012
- 796 Cloud V, Chan Y-L, Grubb J, Budke B, Bishop DK. 2012. Rad51 is an accessory factor for Dmc1-
797 mediated joint molecule formation during meiosis. *Science* **337**:1222–1225.
798 doi:10.1126/science.1219379
- 799 Colaiácovo MP, MacQueen AJ, Martinez-Perez E, McDonald K, Adamo A, La Volpe A,
800 Villeneuve AM. 2003. Synaptonemal Complex Assembly in *C. elegans* Is Dispensable for
801 Loading Strand-Exchange Proteins but Critical for Proper Completion of Recombination.
802 *Developmental Cell*. doi:10.1016/s1534-5807(03)00232-6
- 803 Couteau F, Belzile F, Horlow C, Grandjean O, Vezon D, Doutriaux M-P. 1999. Random
804 Chromosome Segregation without Meiotic Arrest in Both Male and Female Meocytes of a
805 dmc1 Mutant of *Arabidopsis*. *Plant Cell* **11**:1623. doi:10.2307/3871042
- 806 Da Ines O, Degroote F, Goubely C, Amiard S, Gallego ME, White CI. 2013. Meiotic
807 Recombination in *Arabidopsis* Is Catalysed by DMC1, with RAD51 Playing a Supporting
808 Role. *PLoS Genet* **9**:e1003787. doi:10.1371/journal.pgen.1003787
- 809 Dieterich C, Clifton SW, Schuster LN, Chinwalla A, Delehaunty K, Dinkelacker I, Fulton L,
810 Fulton R, Godfrey J, Minx P, Mitreva M, Roeseler W, Tian H, Witte H, Yang S-P, Wilson RK,
811 Sommer RJ. 2008. The *Pristionchus pacificus* genome provides a unique perspective on
812 nematode lifestyle and parasitism. *Nat Genet* **40**:1193–1198. doi:10.1038/ng.227
- 813 Emms DM, Kelly S. 2015. OrthoFinder: solving fundamental biases in whole genome
814 comparisons dramatically improves orthogroup inference accuracy. *Genome Biol* **16**:157.
815 doi:10.1186/s13059-015-0721-2
- 816 Enguita-Marruedo A, Martín-Ruiz M, García E, Gil-Fernández A, Parra MT, Viera A, Rufas JS,
817 Page J. 2019. Transition from a meiotic to a somatic-like DNA damage response during
818 the pachytene stage in mouse meiosis. *PLoS Genet* **15**:e1007439.
819 doi:10.1371/journal.pgen.1007439

- 820 Gray S, Cohen PE. 2016. Control of Meiotic Crossovers: From Double-Strand Break Formation
821 to Designation. *Annu Rev Genet* **50**:175–210. doi:10.1146/annurev-genet-120215-035111
- 822 Grelon M. 2001. AtSPO11-1 is necessary for efficient meiotic recombination in plants. *EMBO J*
823 **20**:589–600. doi:10.1093/emboj/20.3.589
- 824 Harper NC, Rillo R, Jover-Gil S, Assaf ZJ, Bhalla N, Dernburg AF. 2011. Pairing centers recruit a
825 Polo-like kinase to orchestrate meiotic chromosome dynamics in *C. elegans*. *Dev Cell*
826 **21**:934–947. doi:10.1016/j.devcel.2011.09.001
- 827 Hayashi M, Chin GM, Villeneuve AM. 2007. *C. elegans* germ cells switch between distinct
828 modes of double-strand break repair during meiotic prophase progression. *PLoS Genet*
829 **3**:e191. doi:10.1371/journal.pgen.0030191
- 830 Hillers KJ, Jantsch V, Martinez-Perez E, Yanowitz JL. 2017. Meiosis. *WormBook* **2017**:1–43.
831 doi:10.1895/wormbook.1.178.1
- 832 Hoang DT, Chernomor O, von Haeseler A, Minh BQ, Vinh LS. 2018. UFBoot2: Improving the
833 Ultrafast Bootstrap Approximation. *Mol Biol Evol* **35**:518–522. doi:10.1093/molbev/msx281
- 834 Hong EL, Shinohara A, Bishop DK. 2001. *Saccharomyces cerevisiae* Dmc1 protein promotes
835 renaturation of single-strand DNA (ssDNA) and assimilation of ssDNA into homologous
836 super-coiled duplex DNA. *J Biol Chem* **276**:41906–41912. doi:10.1074/jbc.M105563200
- 837 Hong RL, Sommer RJ. 2006. *Pristionchus pacificus*: a well-rounded nematode. *Bioessays*
838 **28**:651–659. doi:10.1002/bies.20404
- 839 Joyce EF, Apostolopoulos N, Beliveau BJ, Wu C-T. 2013. Germline progenitors escape the
840 widespread phenomenon of homolog pairing during *Drosophila* development. *PLoS Genet*
841 **9**:e1004013. doi:10.1371/journal.pgen.1004013
- 842 Kalyanamoorthy S, Minh BQ, Wong TKF, von Haeseler A, Jeremiin LS. 2017. ModelFinder: fast
843 model selection for accurate phylogenetic estimates. *Nat Methods* **14**:587–589.
844 doi:10.1038/nmeth.4285
- 845 Katoh K, Standley DM. 2013. MAFFT multiple sequence alignment software version 7:
846 improvements in performance and usability. *Mol Biol Evol* **30**:772–780.
847 doi:10.1093/molbev/mst010
- 848 Keeney S. 2008. Spo11 and the Formation of DNA Double-Strand Breaks in Meiosis. *Genome*
849 *Dyn Stab* **2**:81–123. doi:10.1007/7050_2007_026
- 850 Keeney S, Giroux CN, Kleckner N. 1997. Meiosis-specific DNA double-strand breaks are
851 catalyzed by Spo11, a member of a widely conserved protein family. *Cell* **88**:375–384.
- 852 Kim Y, Kostow N, Dernburg AF. 2015. The Chromosome Axis Mediates Feedback Control of
853 CHK-2 to Ensure Crossover Formation in *C. elegans*. *Dev Cell* **35**:247–261.
854 doi:10.1016/j.devcel.2015.09.021
- 855 Kocot KM, Citarella MR, Moroz LL, Halanych KM. 2013. PhyloTreePruner: A Phylogenetic Tree-
856 Based Approach for Selection of Orthologous Sequences for Phylogenomics. *Evol*
857 *Bioinform Online* **9**:429–435. doi:10.4137/EBO.S12813
- 858 Labella S, Woglar A, Jantsch V, Zetka M. 2011. Polo kinases establish links between meiotic
859 chromosomes and cytoskeletal forces essential for homolog pairing. *Dev Cell* **21**:948–958.
860 doi:10.1016/j.devcel.2011.07.011
- 861 Letunic I, Bork P. 2016. Interactive tree of life (iTOL) v3: an online tool for the display and
862 annotation of phylogenetic and other trees. *Nucleic Acids Res* **44**:W242–5.
863 doi:10.1093/nar/gkw290

- 864 Li Z, Golub EI, Gupta R, Radding CM. 1997. Recombination activities of HsDmc1 protein, the
865 meiotic human homolog of RecA protein. *Proc Natl Acad Sci US A* **94**:11221–11226.
- 866 Lo T-W, Pickle CS, Lin S, Ralston EJ, Gurling M, Schartner CM, Bian Q, Doudna JA, Meyer BJ.
867 2013. Precise and heritable genome editing in evolutionarily diverse nematodes using
868 TALENs and CRISPR/Cas9 to engineer insertions and deletions. *Genetics* **195**:331–348.
869 doi:10.1534/genetics.113.155382
- 870 Lui DY, Colaiácovo MP. 2012. Meiotic Development in *Caenorhabditis elegans* Advances in
871 Experimental Medicine and Biology. pp. 133–170. doi:10.1007/978-1-4614-4015-4_6
- 872 MacQueen AJ, Colaiácovo MP, McDonald K, Villeneuve AM. 2002. Synapsis-dependent and -
873 independent mechanisms stabilize homolog pairing during meiotic prophase in *C. elegans*.
874 *Genes Dev* **16**:2428–2442. doi:10.1101/gad.1011602
- 875 MacQueen AJ, Phillips CM, Bhalla N, Weiser P, Villeneuve AM, Dernburg AF. 2005.
876 Chromosome sites play dual roles to establish homologous synapsis during meiosis in *C.*
877 *elegans*. *Cell* **123**:1037–1050. doi:10.1016/j.cell.2005.09.034
- 878 Martinez-Perez E, Colaiácovo MP. 2009. Distribution of meiotic recombination events: talking
879 to your neighbors. *Curr Opin Genet Dev* **19**:105–112. doi:10.1016/j.gde.2009.02.005
- 880 Martin JS, Winkelmann N, Petalcorin MIR, McIlwraith MJ, Boulton SJ. 2005. RAD-51-
881 dependent and -independent roles of a *Caenorhabditis elegans* BRCA2-related protein
882 during DNA double-strand break repair. *Mol Cell Biol* **25**:3127–3139.
883 doi:10.1128/MCB.25.8.3127-3139.2005
- 884 Masson JY, Davies AA, Hajibagheri N, Van Dyck E, Benson FE, Stasiak AZ, Stasiak A, West SC.
885 1999. The meiosis-specific recombinase hDmc1 forms ring structures and interacts with
886 hRad51. *EMBO J* **18**:6552–6560. doi:10.1093/emboj/18.22.6552
- 887 Nadarajan S, Lambert TJ, Altendorfer E, Gao J, Blower MD, Waters JC, Colaiácovo MP. 2017.
888 Polo-like kinase-dependent phosphorylation of the synaptonemal complex protein SYP-4
889 regulates double-strand break formation through a negative feedback loop. *Elife* **6**.
890 doi:10.7554/eLife.23437
- 891 Namai S, Sugimoto A. 2018. Transgenesis by microparticle bombardment for live imaging of
892 fluorescent proteins in *Pristionchus pacificus* germline and early embryos. *Dev Genes Evol*
893 **228**:75–82. doi:10.1007/s00427-018-0605-z
- 894 Nguyen L-T, Schmidt HA, von Haeseler A, Minh BQ. 2015. IQ-TREE: a fast and effective
895 stochastic algorithm for estimating maximum-likelihood phylogenies. *Mol Biol Evol*
896 **32**:268–274. doi:10.1093/molbev/msu300
- 897 Pattabiraman D, Roelens B, Woglar A, Villeneuve AM. 2017. Meiotic recombination modulates
898 the structure and dynamics of the synaptonemal complex during *C. elegans* meiosis.
899 doi:10.1101/110064
- 900 Penkner AM, Fridkin A, Gloggnitzer J, Baudrimont A, Machacek T, Woglar A, Csaszar E,
901 Pasierbek P, Ammerer G, Gruenbaum Y, Jantsch V. 2009. Meiotic chromosome homology
902 search involves modifications of the nuclear envelope protein Matefin/SUN-1. *Cell*
903 **139**:920–933. doi:10.1016/j.cell.2009.10.045
- 904 Phillips CM, Dernburg AF. 2006. A family of zinc-finger proteins is required for chromosome-
905 specific pairing and synapsis during meiosis in *C. elegans*. *Dev Cell* **11**:817–829.
906 doi:10.1016/j.devcel.2006.09.020
- 907 Phillips CM, Wong C, Bhalla N, Carlton PM, Weiser P, Meneely PM, Dernburg AF. 2005. HIM-8

- 908 binds to the X chromosome pairing center and mediates chromosome-specific meiotic
909 synapsis. *Cell* **123**:1051–1063. doi:10.1016/j.cell.2005.09.035
- 910 Pires-daSilva A. 2004. Conservation of the global sex determination gene *tra-1* in distantly
911 related nematodes. *Genes Dev* **18**:1198–1208. doi:10.1101/gad.293504
- 912 Pittman DL, Cobb J, Schimenti KJ, Wilson LA, Cooper DM, Brignull E, Handel MA, Schimenti
913 JC. 1998. Meiotic Prophase Arrest with Failure of Chromosome Synapsis in Mice Deficient
914 for *Dmc1*, a Germline-Specific RecA Homolog. *Mol Cell* **1**:697–705. doi:10.1016/s1097-
915 2765(00)80069-6
- 916 Rinaldo C, Bazzicalupo P, Ederle S, Hilliard M, La Volpe A. 2002. Roles for *Caenorhabditis*
917 *elegans rad-51* in meiosis and in resistance to ionizing radiation during development.
918 *Genetics* **160**:471–479.
- 919 Rockmill B, Sym M, Scherthan H, Roeder GS. 1995. Roles for two RecA homologs in promoting
920 meiotic chromosome synapsis. *Genes Dev* **9**:2684–2695. doi:10.1101/gad.9.21.2684
- 921 Rödelberger C, Meyer JM, Prabh N, Lanz C, Bemm F, Sommer RJ. 2017. Single-Molecule
922 Sequencing Reveals the Chromosome-Scale Genomic Architecture of the Nematode
923 Model Organism *Pristionchus pacificus*. *Cell Rep* **21**:834–844.
924 doi:10.1016/j.celrep.2017.09.077
- 925 Rog O, Dernburg AF. 2013. Chromosome pairing and synapsis during *Caenorhabditis elegans*
926 meiosis. *Current Opinion in Cell Biology*. doi:10.1016/j.ceb.2013.03.003
- 927 Rubin T, Christophorou N, Huynh J-R. 2016. How to pre-pair chromosomes for meiosis. *Cell*
928 *Cycle* **15**:609–610. doi:10.1080/15384101.2015.1131524
- 929 Rudel D, Riebesell M, Sommer RJ. 2005. Gonadogenesis in *Pristionchus pacificus* and organ
930 evolution: development, adult morphology and cell–cell interactions in the hermaphrodite
931 gonad. *Developmental Biology*. doi:10.1016/j.ydbio.2004.09.021
- 932 Sato A, Isaac B, Phillips CM, Rillo R, Carlton PM, Wynne DJ, Kasad RA, Dernburg AF. 2009.
933 Cytoskeletal forces span the nuclear envelope to coordinate meiotic chromosome pairing
934 and synapsis. *Cell* **139**:907–919. doi:10.1016/j.cell.2009.10.039
- 935 Smolikov S, Eizinger A, Schild-Prufert K, Hurlburt A, McDonald K, Engebrecht J, Villeneuve
936 AM, Colaiácovo MP. 2007. SYP-3 restricts synaptonemal complex assembly to bridge
937 paired chromosome axes during meiosis in *Caenorhabditis elegans*. *Genetics* **176**:2015–
938 2025. doi:10.1534/genetics.107.072413
- 939 Smolikov S, Schild-Prüfert K, Colaiácovo MP. 2009. A yeast two-hybrid screen for SYP-3
940 interactors identifies SYP-4, a component required for synaptonemal complex assembly
941 and chiasma formation in *Caenorhabditis elegans* meiosis. *PLoS Genet* **5**:e1000669.
942 doi:10.1371/journal.pgen.1000669
- 943 Sommer RJ. 2015. *Pristionchus pacificus*: A Nematode Model for Comparative and
944 Evolutionary Biology. BRILL.
- 945 Sommer RJ, Carta LK, Kim S-Y, Sternburg PW. 1996. Morphological, genetic and molecular
946 description of *Pristionchus pacificus* sp. N. (Nematoda: Neodiplogastridae). *Fundam. Appl.*
947 *Nematol.* **19**: 511-521
- 948 Srinivasan J, Sinz W, Jesse T, Wiggers-Perebolte L, Jansen K, Buntjer J, van der Meulen M,
949 Sommer RJ. 2003. An integrated physical and genetic map of the nematode *Pristionchus*
950 *pacificus*. *Mol Genet Genomics* **269**:715–722. doi:10.1007/s00438-003-0881-8
- 951 Srinivasan J, Sinz W, Lanz C, Brand A, Nandakumar R, Raddatz G, Witte H, Keller H, Kipping I,

- 952 Pires-daSilva A, Jesse T, Millare J, de Both M, Schuster SC, Sommer RJ. 2002. A bacterial
953 artificial chromosome-based genetic linkage map of the nematode *Pristionchus pacificus*.
954 *Genetics* **162**:129–134.
- 955 Vader G, Musacchio A. 2014. HORMA domains at the heart of meiotic chromosome dynamics.
956 *Dev Cell* **31**:389–391. doi:10.1016/j.devcel.2014.11.009
- 957 Villeneuve AM, Hillers KJ. 2001. Whence meiosis? *Cell* **106**:647–650.
- 958 Witte H, Moreno E, Rödelberger C, Kim J, Kim J-S, Streit A, Sommer RJ. 2015. Gene
959 inactivation using the CRISPR/Cas9 system in the nematode *Pristionchus pacificus*. *Dev*
960 *Genes Evol* **225**:55–62. doi:10.1007/s00427-014-0486-8
- 961 Yokoo R, Zawadzki KA, Nabeshima K, Drake M, Arur S, Villeneuve AM. 2012. COSA-1 reveals
962 robust homeostasis and separable licensing and reinforcement steps governing meiotic
963 crossovers. *Cell* **149**:75–87. doi:10.1016/j.cell.2012.01.052
- 964 Yoshida K, Kondoh G, Matsuda Y, Habu T, Nishimune Y, Morita T. 1998. The Mouse RecA -like
965 Gene Dmc1 Is Required for Homologous Chromosome Synapsis during Meiosis. *Mol Cell*
966 **1**:707–718. doi:10.1016/s1097-2765(00)80070-2
- 967 Zhang L, Köhler S, Rillo-Bohn R, Dernburg AF. 2018. A compartmentalized signaling network
968 mediates crossover control in meiosis. *Elife* **7**. doi:10.7554/eLife.30789
- 969 Zickler D, Kleckner N. 1999. Meiotic chromosomes: integrating structure and function. *Annu*
970 *Rev Genet* **33**:603–754. doi:10.1146/annurev.genet.33.1.603

Figure 1

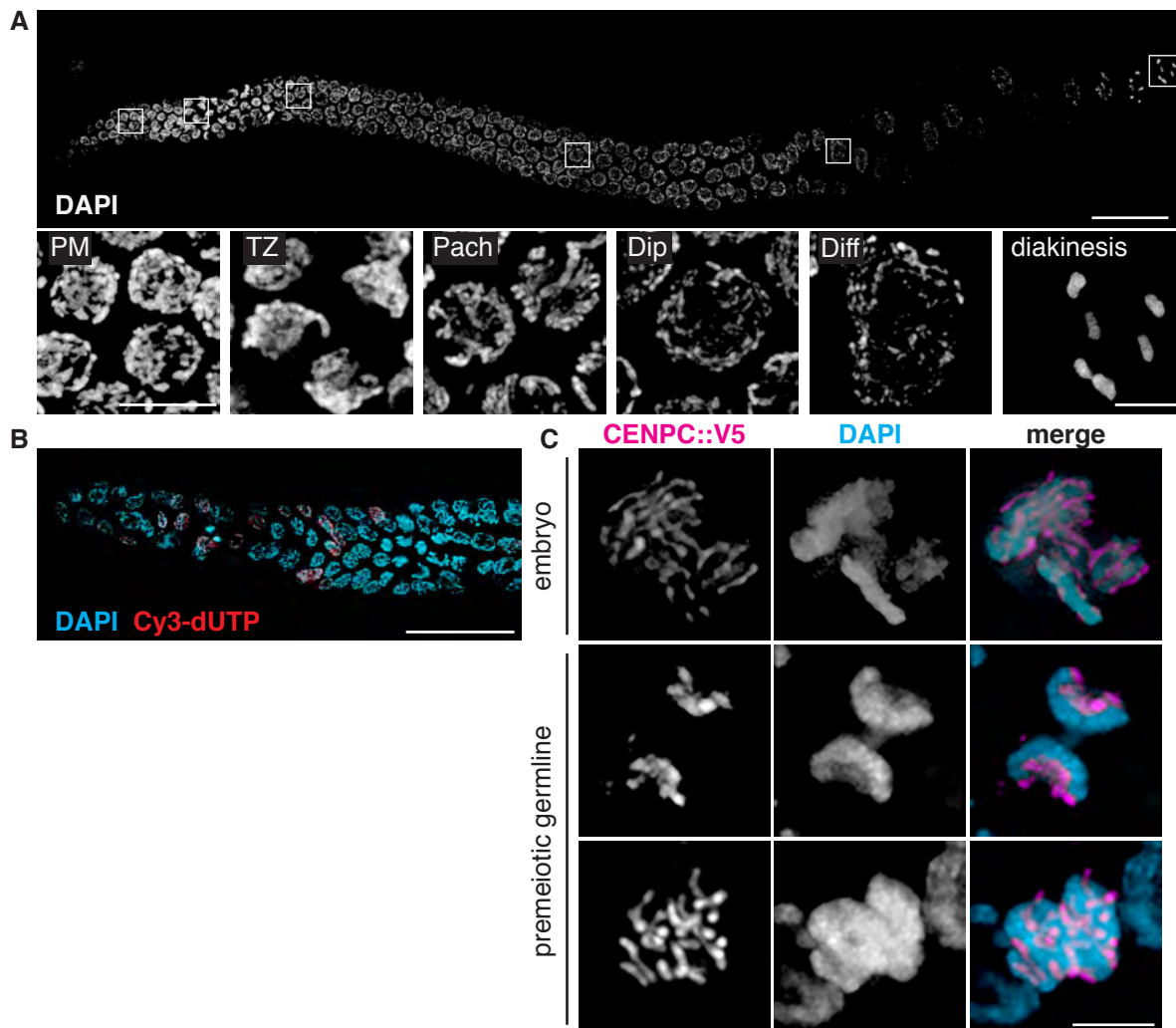


Figure 2

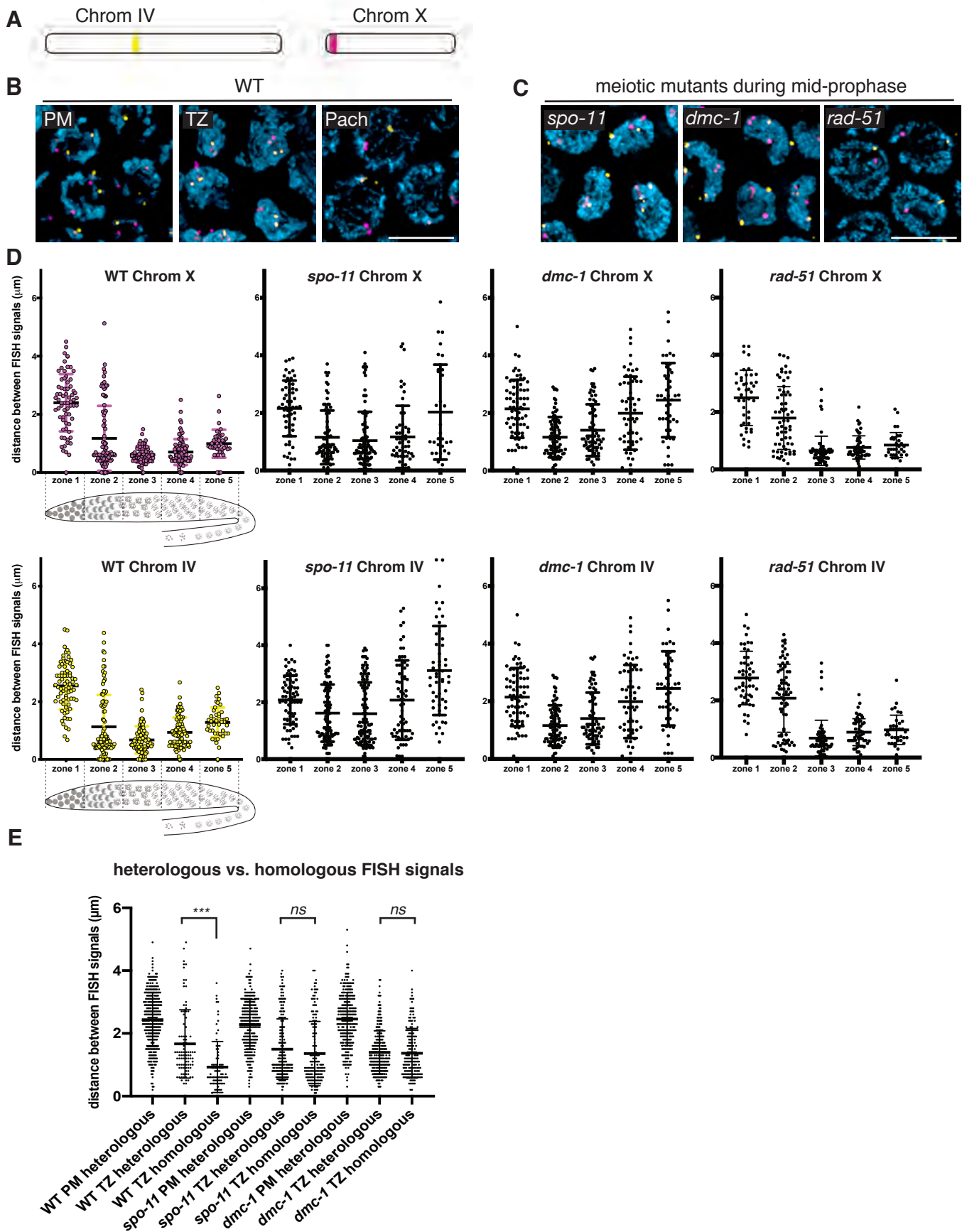


Figure 2- figure supplement 1

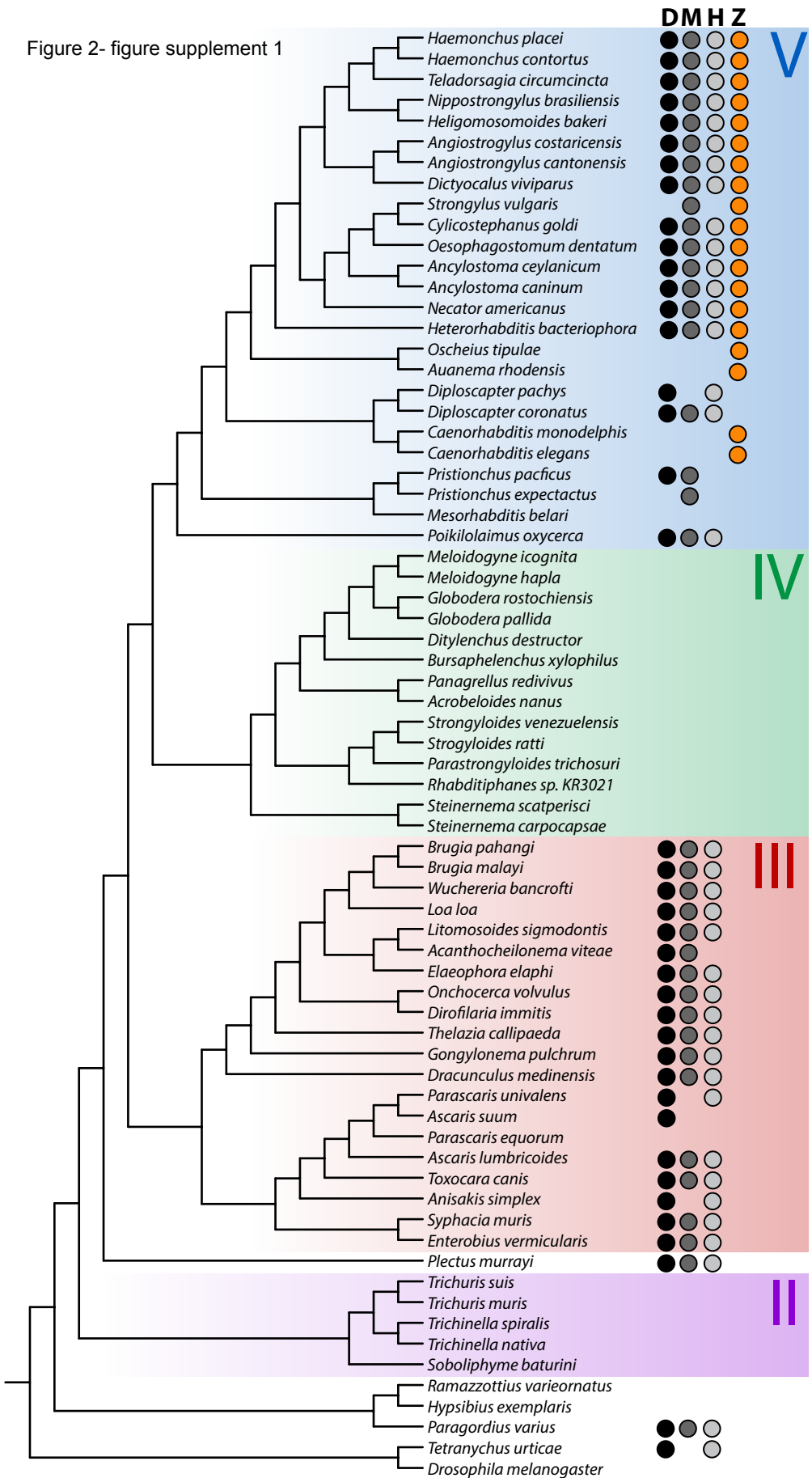


Figure 2- figure supplement 2

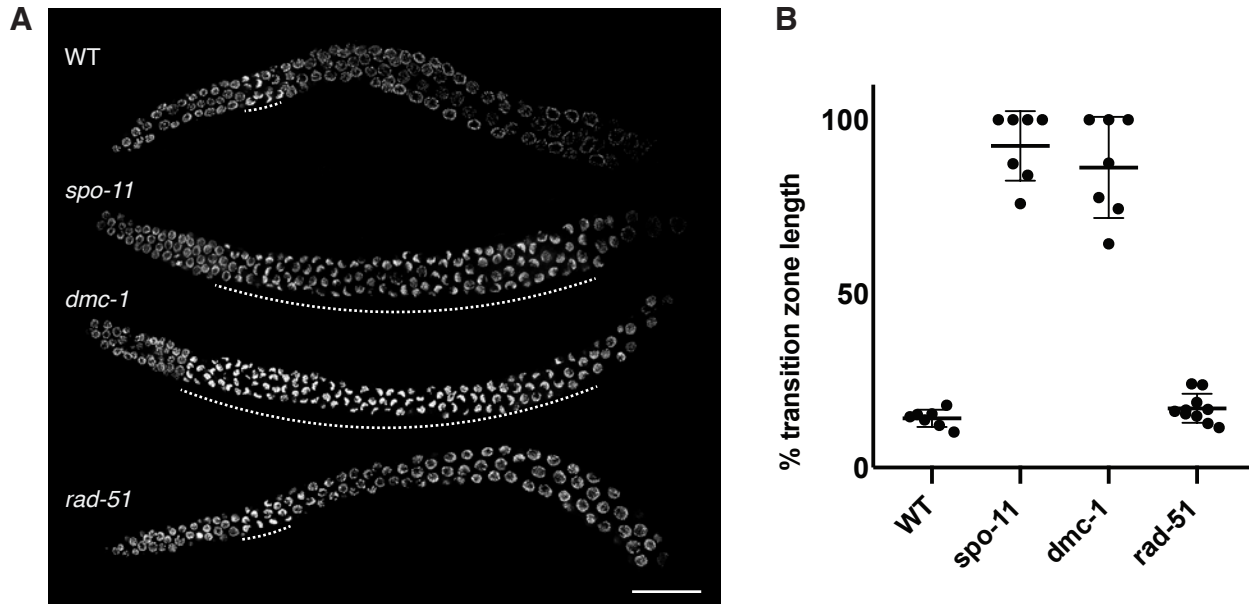


Figure 3

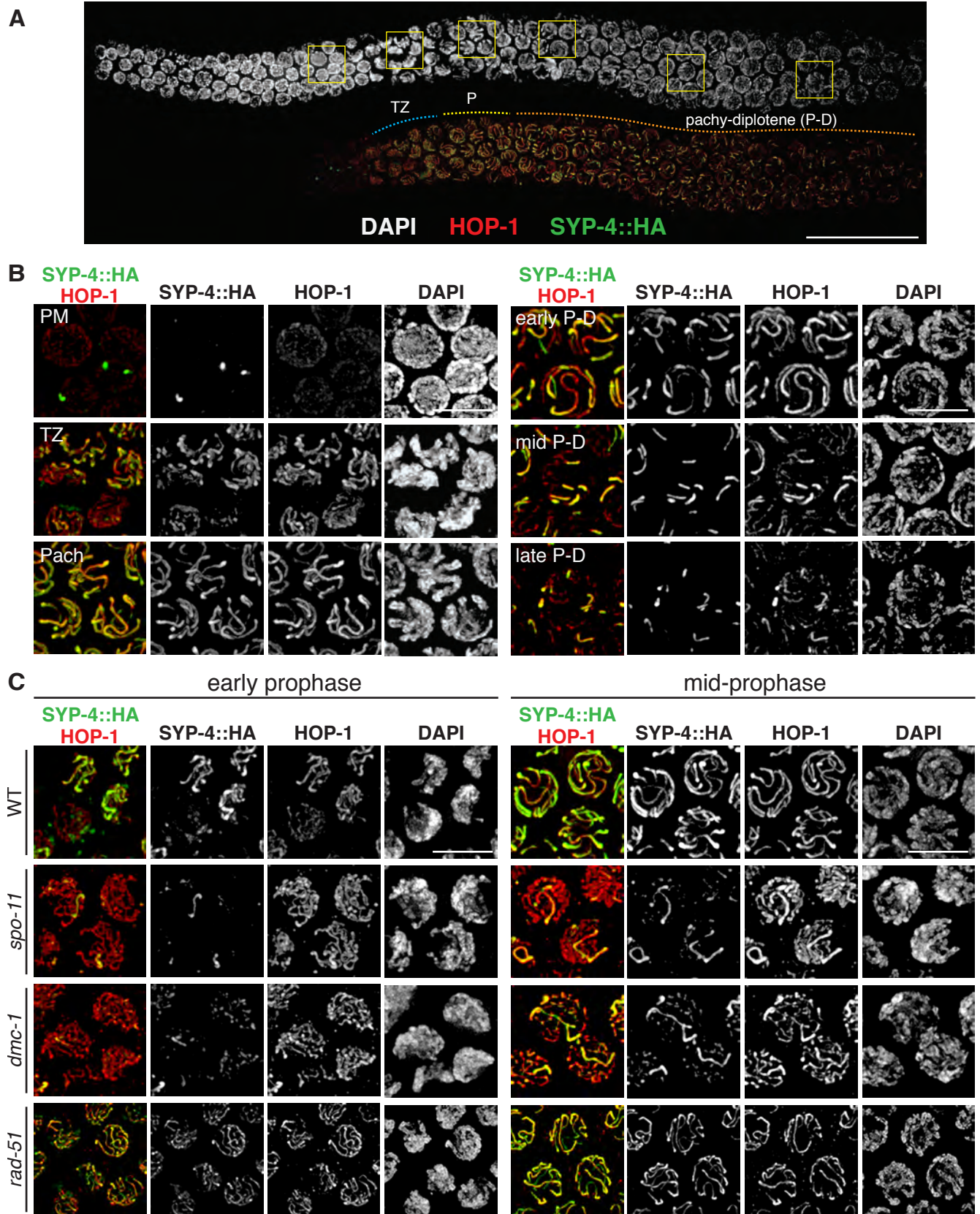


Figure 4

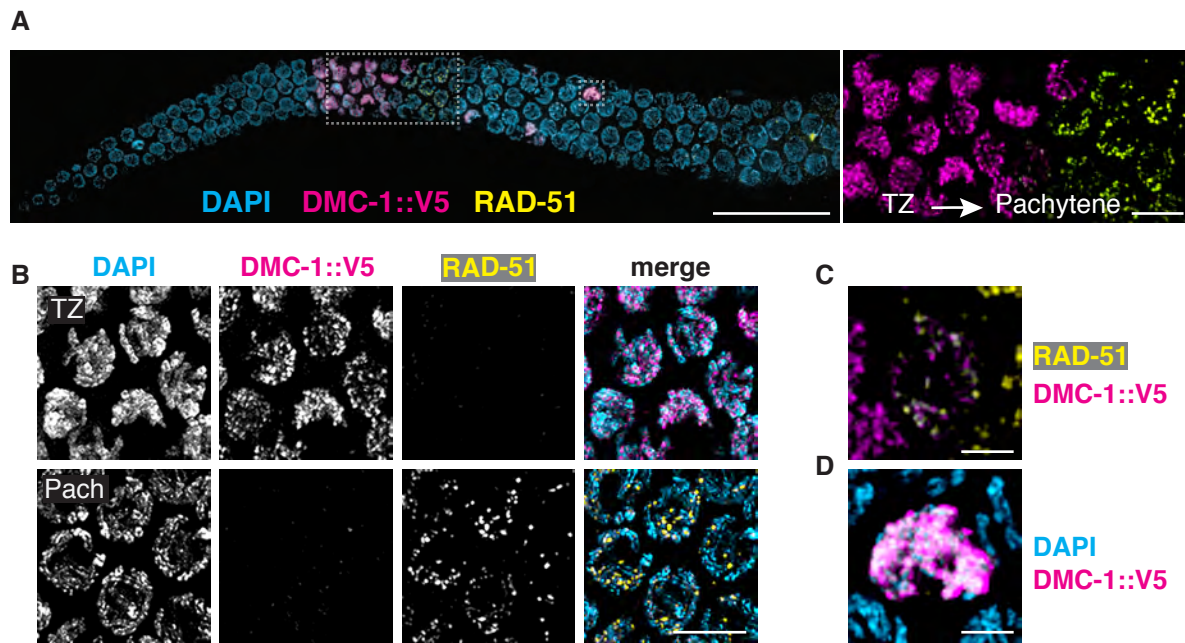


Figure 4- figure supplement 1

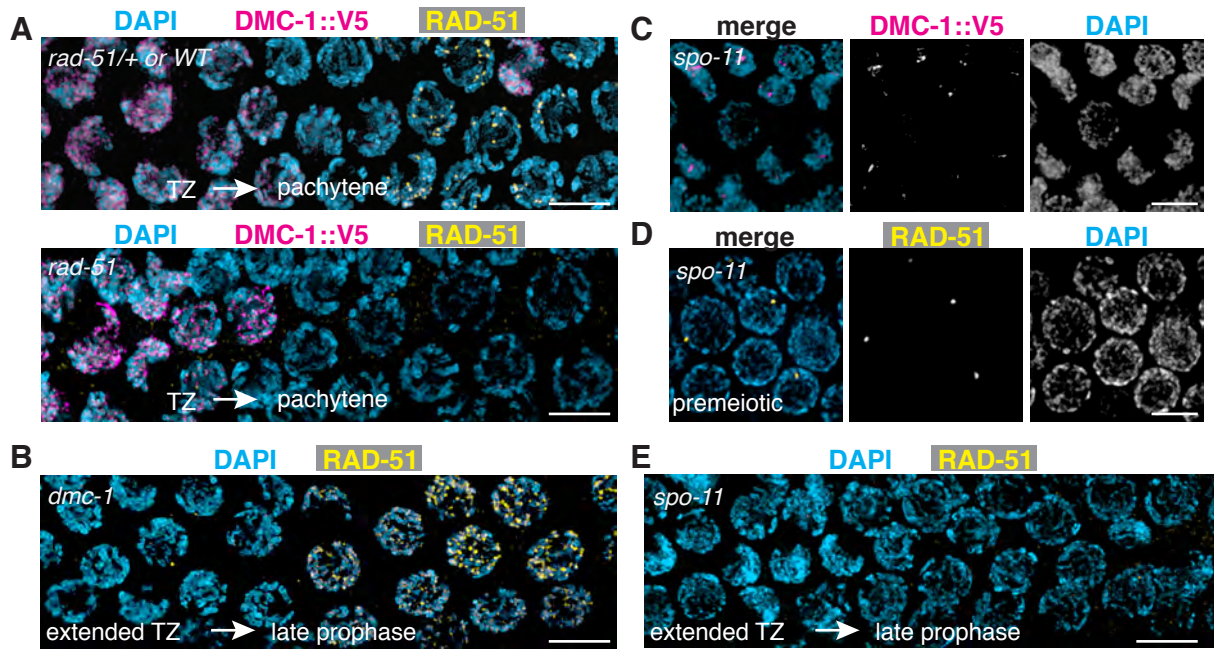


Figure 5

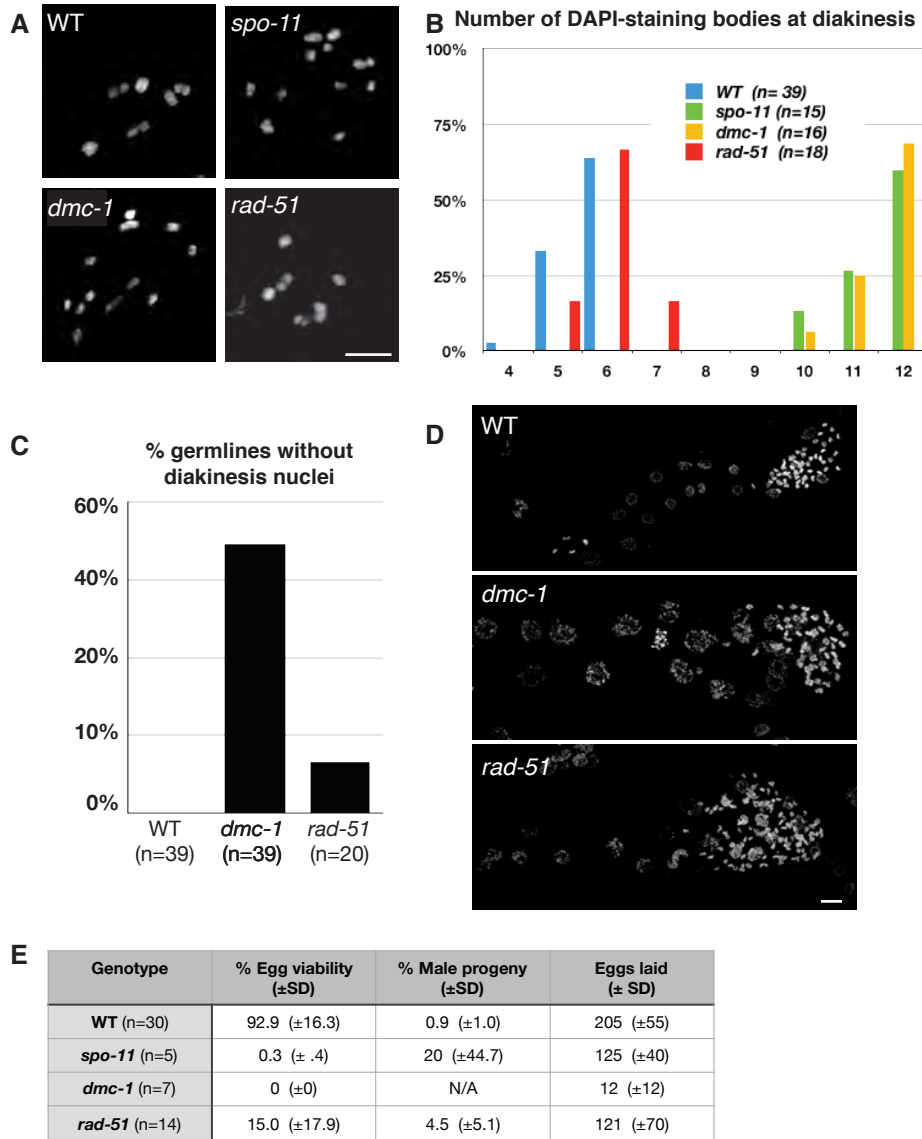
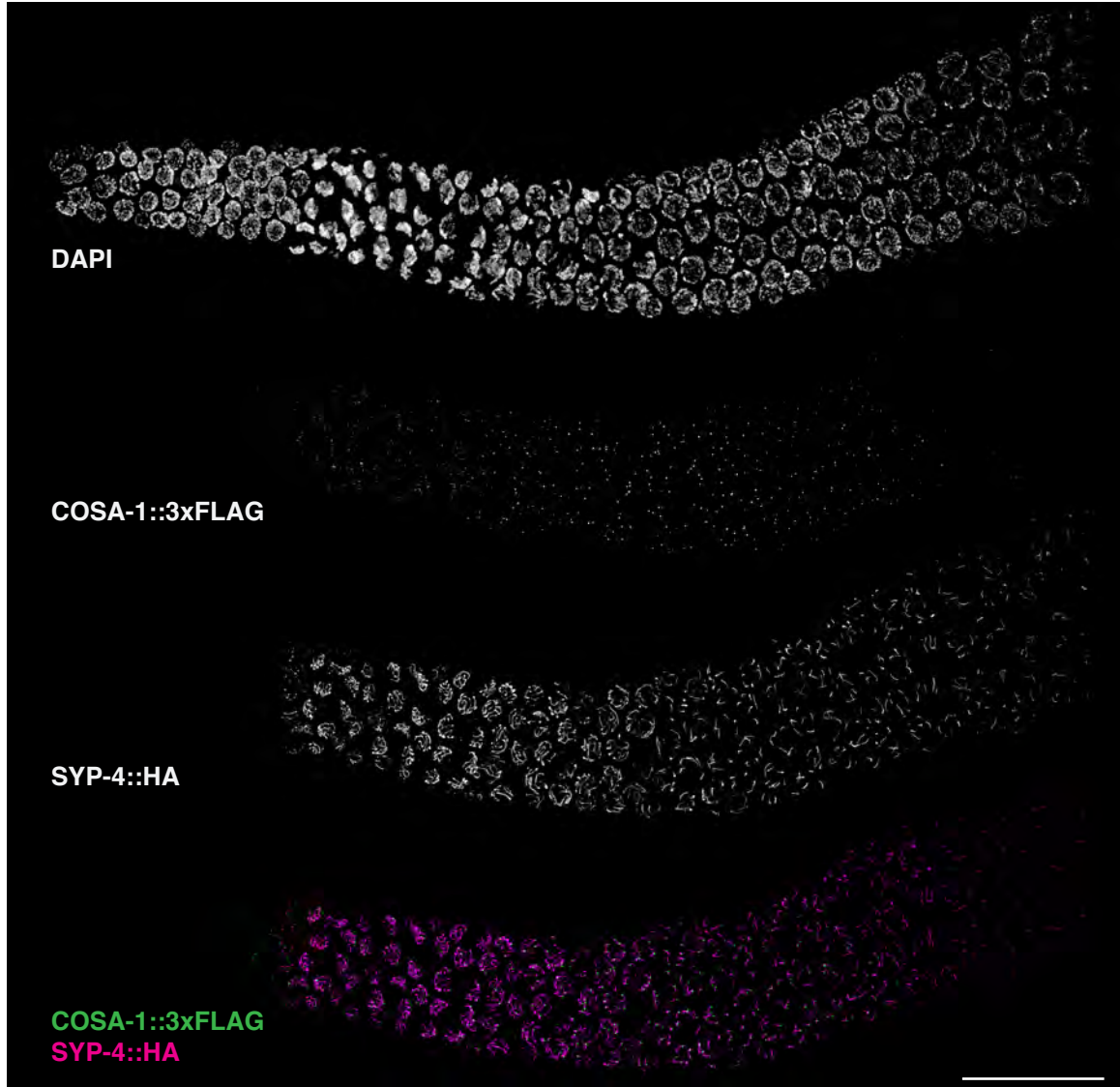
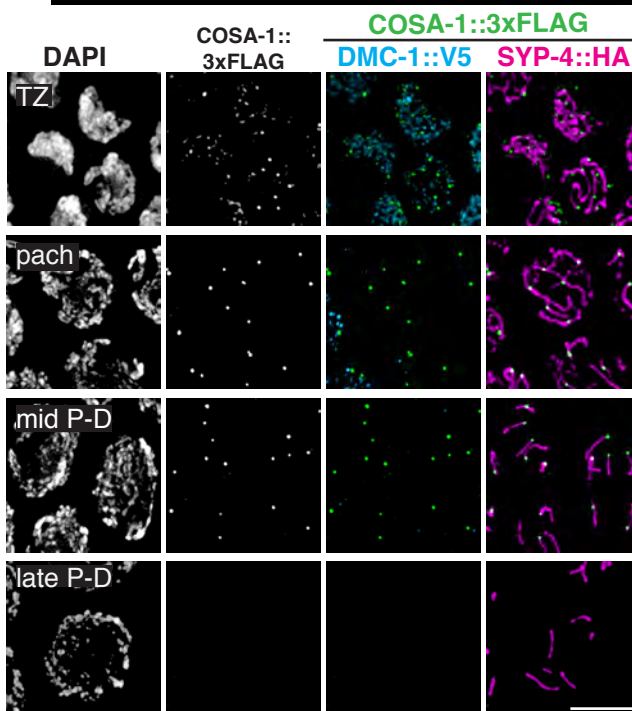


Figure 6

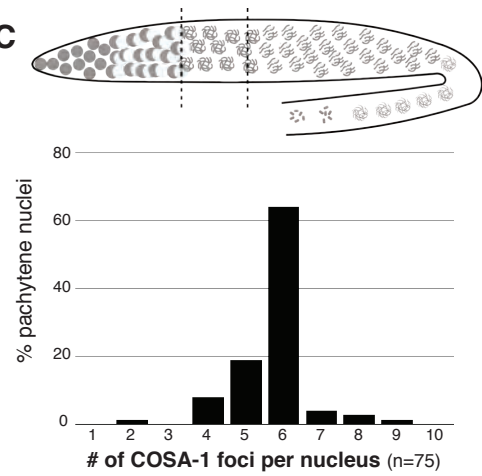
A



B



C



D

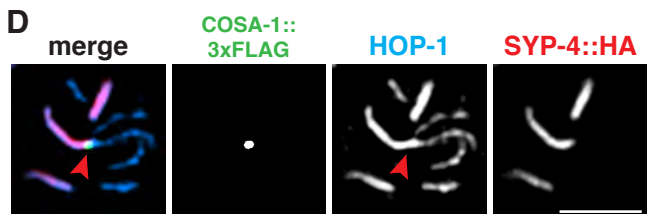


Figure 6- figure supplement 1

A

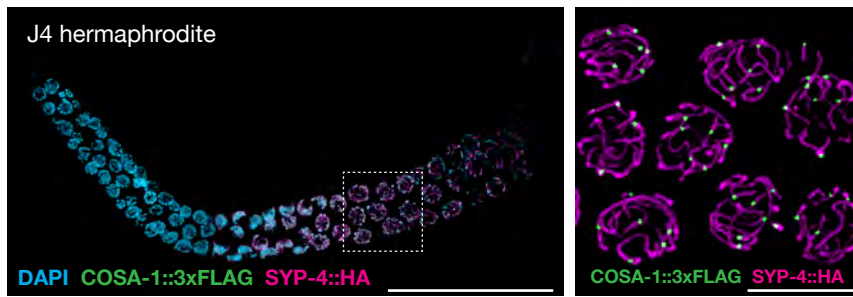


Figure 7

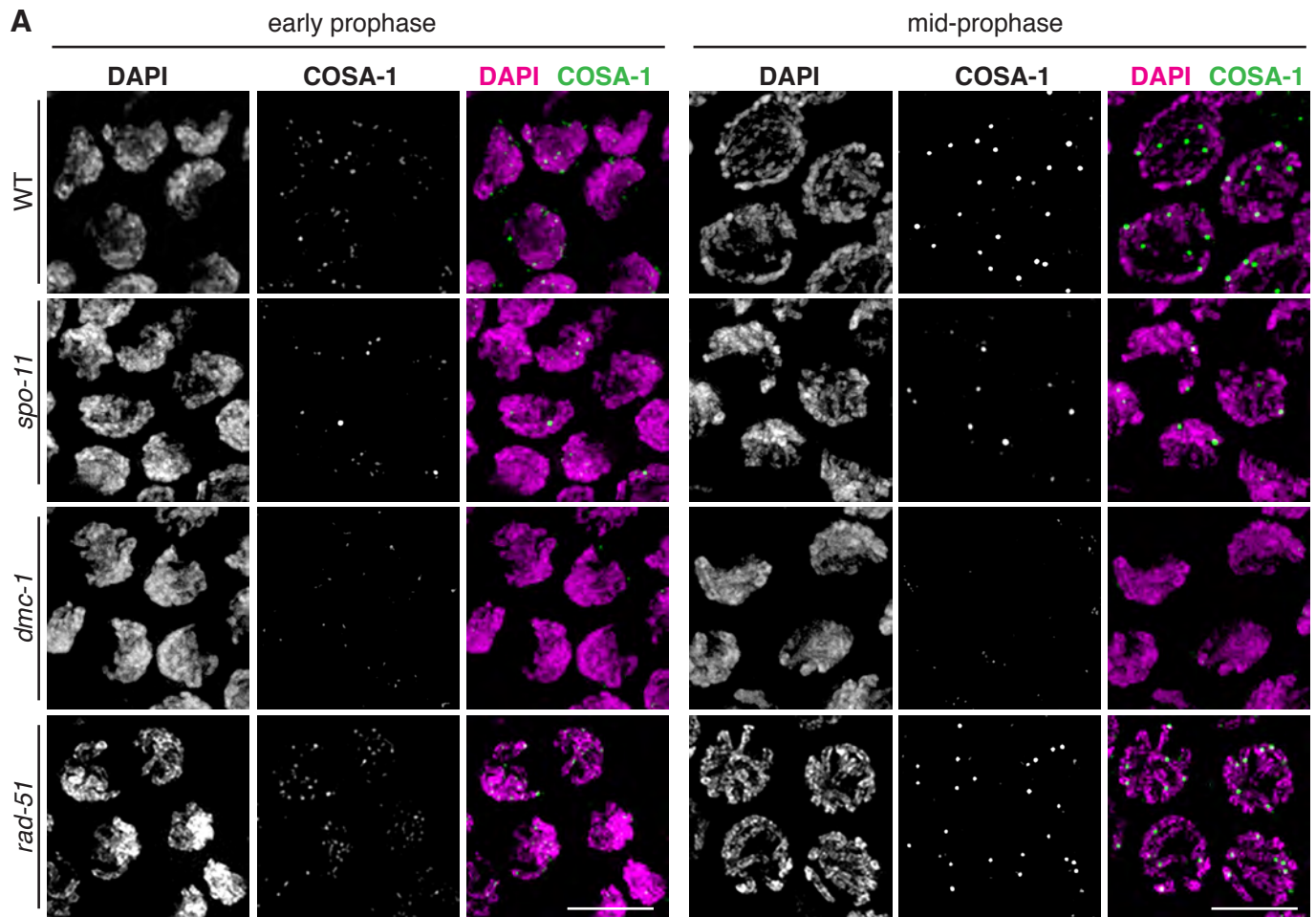


Table S1

| Strain | Allele | guide RNA target sequence (PAM sequence underlined) | ssDNA template | genotyping primer sequences |
|-----------------------|---------------|--|--|--|
| <i>cenpc::V5</i> | <i>ie1007</i> | ATGAAGAGATGGATTATAGT <u>AGG</u> | GGATATTAATAAGGGGGTAAAATTGTACATCGCAAAGGA TGAGGAGTCATTTAATTCATCTTACTATAATCCATCTCTTCAG GTGGAGTCGAGTCCAAGAAGTGGGTTTGAATTGGCTTTC CAGATCCGGCTCCTTCATTCTCTTCATCGAACTCTTCCACTT CCTTCTCCTTCTGCTCTTTTCTCTTCTTGT | (f)TTTCTCCAGGAGTGGTTATCG (r)ACATCGCAAAGGATGAGGAG |
| <i>cosa-1::3xflag</i> | <i>ie1003</i> | CTTTATTCTTCATTTTACAGT <u>GG</u> | GATCATCCCAGGGAGAGAACGACCTACCCAAACAGAGATCA TAGATCTAATTATCCACTGGGAGCCGGATCTGATTATAAAGA CCATGATGGAGACTATAAGGATCACGATATTGATTACAAAGA CGATGATGATAAATAAATGAAGAATAAAGAGATTAAATTTAT GTTTGTGTTTCGTTTTTGAATTACTGCTTTG | (f)ACGACCTACCCAAACAGAGA (r)CGGATGTGGAAAGACGTACC |
| <i>dmc-1</i> mutant | <i>ie1005</i> | TTCGATAAGCTGCTTGGAGG <u>I</u> GG | ATTTAATTGTAACATTCAGACATCCAGTTGATCAACTAACCTC CGTTATTGCCTGACTTTTCGATTCCACCactagtTCCAAGCAG CTTATCGAATTCAACACTTCCAGTGGAGATTTTAAAGACTTG CTTGCGTCGTGAACACACT | (f)GGACTCTCGGAGGCTAAAGT (r)ATTCTCGAGCATTGCTTCT |
| <i>dmc-1::V5</i> | <i>ie1001</i> | GCAACGTTTGCCATTGCAGC <u>AGG</u> | GATAAAACATGATCTTTTGTCTTCATAATTGATTAGGTGGAG TCGAGTCCAAGAAGTGGGTTTGAATTGGCTTTCCATCCTT TGCATCGACAATTCCTCCTGCGGCGATGGCAAACGTTGCTT CGTTCTCAGGCATATC | (f)TGCCTGAGAACGAAGCAACG (r)ACATGAGATGGCACAAGGAC |
| <i>rad-51</i> mutant | <i>ie1006</i> | GTCGAGAACGAGGAGAATGCC <u>GG</u> | ATTTATTGGTTACCTCAAGGGACATGATGGACTGGCAGGCG AGTCCGGCATACTAGTTTCTCCTCGTTCTCGACATCAGCGT CGACGTGCGCCATTTGAGCGGACAT | (f)TTCTAGTGACGCGTGTGTT (r)ACGAATCCTCGTTGCTGAAG |
| <i>spo-11</i> mutant | <i>ie1004</i> | ATTCAGAACTTGGCAGAGAT <u>CGG</u> | ACAAACATCTTTTTGCACGACAGGATTCTCTCAATCGATCAG TTTCCGATaactagtaCTCTGCCAAGTTCTGAATATGCAAAGAT GTCAAGTCAATGTGGTAAGT | (f)GGAAATCCTTCGTTCTCACTATGG (r)GTCTCAATATCAGACAATTTATTCCG |
| <i>syp-4::HA</i> | <i>ie1002</i> | GGAGGAGAATTCAACTTCTT <u>CGG</u> | CAAATGGAGGTGGCGGCGGGGGAGGAGGAGAGTTAATTT TTTTGGTTTTTACCCCTACGATGTCCCAGATTATGCTTAAAC CAATTTTTTCGAGCTTGGTGAATGTATCCA | (f)CCCGTTGATGATGCTACCAG (r)GATACATTACCCAAGCTCGAA |

Table S2

| Species | Prefix | Source | BioProject |
|--------------------------------------|---------------|--|-------------------|
| <i>Acanthocheilonema viteae</i> | AVITAE | WormBase ParaSite | PRJEB4306 |
| <i>Acrobeloides nanus</i> | ANANUS | WormBase ParaSite | PRJEB26554 |
| <i>Ancylostoma caninum</i> | ACANIN | WormBase ParaSite | PRJNA72585 |
| <i>Ancylostoma ceylanicum</i> | ACEYLA | WormBase ParaSite | PRJNA231479 |
| <i>Angiostrongylus cantonensis</i> | ACANTO | WormBase ParaSite | PRJEB493 |
| <i>Angiostrongylus costaricensis</i> | ACOSTA | WormBase ParaSite | PRJEB494 |
| <i>Anisakis simplex</i> | ASIMPL | WormBase ParaSite | PRJEB496 |
| <i>Ascaris lumbricoides</i> | ALUMBR | WormBase ParaSite | PRJEB4950 |
| <i>Ascaris suum</i> | ASSUUM | WormBase ParaSite | PRJNA62057 |
| <i>Auanema rhodensis</i> | ARHODE | - | PRJEB29492 |
| <i>Brugia malayi</i> | BMALAY | WormBase ParaSite | PRJNA10729 |
| <i>Brugia pahangi</i> | BPAHAN | WormBase ParaSite | PRJEB497 |
| <i>Bursaphelenchus xylophilus</i> | BXYLOP | WormBase ParaSite | PRJEA64437 |
| <i>Caenorhabditis elegans</i> | CELEGA | WormBase ParaSite | PRJNA13758 |
| <i>Caenorhabditis monodelphis</i> | CMONOD | caenorhabditis.org | PRJEB7905 |
| <i>Cylicostephanus goldi</i> | CGOLDI | WormBase ParaSite | PRJEB498 |
| <i>Dictyocaulus viviparus</i> | DVIVIP | WormBase ParaSite | PRJNA72587 |
| <i>Diploscapter coronatus</i> | DCORON | WormBase ParaSite | PRJDB3143 |
| <i>Diploscapter pachys</i> | DPACHY | WormBase ParaSite | PRJNA280107 |
| <i>Dirofilaria immitis</i> | DIMMIT | WormBase ParaSite | PRJEB1797 |
| <i>Ditylenchus destructor</i> | DDESTR | WormBase ParaSite | PRJNA312427 |
| <i>Dracunculus medinensis</i> | DMEDIN | WormBase ParaSite | PRJEB500 |
| <i>Drosophila melanogaster</i> | DMELAN | Ensembl | BDGP6 |
| <i>Elaeophora elaphi</i> | EELAPH | WormBase ParaSite | PRJEB502 |
| <i>Enterobius vermicularis</i> | EVERMI | WormBase ParaSite | PRJEB503 |
| <i>Globodera pallida</i> | GPALLI | WormBase ParaSite | PRJEB123 |
| <i>Globodera rostochiensis</i> | GROSTO | WormBase ParaSite | PRJEB13504 |
| <i>Gongylonema pulchrum</i> | GPULCH | WormBase ParaSite | PRJEB505 |
| <i>Paragordius varius</i> | GORDSP | - | - |
| <i>Haemonchus contortus</i> | HCONTO | WormBase ParaSite | PRJEB506 |
| <i>Haemonchus placei</i> | HPLACE | WormBase ParaSite | PRJEB509 |
| <i>Heligmosomoides bakeri</i> | HBAKEI | - | PRJEB15396 |
| <i>Heterorhabditis bacteriophora</i> | HBACTE | caenorhabditis.org | PRJNA13977 |
| <i>Hypsibius exemplaris</i> | HEXEMP | tardigrades.org | PRJNA360553 |
| <i>Litomosoides sigmodontis</i> | LSIGMO | WormBase ParaSite | PRJEB3075 |
| <i>Loa loa</i> | LOALOA | WormBase ParaSite | PRJNA246086 |
| <i>Meloidogyne hapla</i> | MHAPLA | WormBase ParaSite | PRJNA29083 |
| <i>Meloidogyne incognita</i> | MINCOG | WormBase ParaSite | PRJEA28837 |
| <i>Mesorhabditis belari</i> | MBELAR | caenorhabditis.org | PRJEB30104 |
| <i>Necator americanus</i> | NAMERI | WormBase ParaSite | PRJNA72135 |
| <i>Nippostrongylus brasiliensis</i> | NBRASS | WormBase ParaSite | PRJEB511 |
| <i>Oesophagostomum dentatum</i> | ODENTA | WormBase ParaSite | PRJNA72579 |
| <i>Onchocerca volvulus</i> | OVOLVO | WormBase ParaSite | PRJEB513 |
| <i>Oschieus tipulae</i> | OTIPUL | caenorhabditis.org | PRJEB15512 |
| <i>Panagrellus redivivus</i> | PREDIV | WormBase ParaSite | PRJNA186477 |
| <i>Parascaris equorum</i> | PEQUOR | WormBase ParaSite | PRJEB514 |
| <i>Parascaris univalens</i> | PUNIVA | WormBase ParaSite | PRJNA386823 |
| <i>Parastrongyloides trichosuri</i> | PTRICH | WormBase ParaSite | PRJEB515 |
| <i>Plectus murrayi</i> | PMURRA | ngenomes.org | - |
| <i>Poikilolaimus oxycercus</i> | POXYCE | caenorhabditis.org | - |
| <i>Pristionchus exspectatus</i> | PEXPEC | WormBase ParaSite | PRJEB6009 |
| <i>Pristionchus pacificus</i> | PPACIF | WormBase ParaSite | PRJNA12644 |
| <i>Ramazzottius varieornatus</i> | RVARIE | tardigrades.org | PRJDB1451 |
| <i>Rhabditophanes sp. KR3021</i> | KR3021 | WormBase ParaSite | PRJEB1297 |
| <i>Soboliphyme baturini</i> | SBATUR | WormBase ParaSite | PRJEB516 |
| <i>Steinernema carpocapsae</i> | SCARPO | WormBase ParaSite | PRJNA202318 |
| <i>Steinernema scapterisci</i> | SSCAPT | WormBase ParaSite | PRJNA204942 |
| <i>Strongyloides ratti</i> | SRATTI | WormBase ParaSite | PRJEB125 |

| Species | Prefix | Source | BioProject |
|------------------------------------|---------------|-------------------|-------------------|
| <i>Strongyloides venezuelensis</i> | SVENEZ | WormBase ParaSite | PRJEB530 |
| <i>Strongylus vulgaris</i> | SVULGA | WormBase ParaSite | PRJEB531 |
| <i>Syphacia muris</i> | SMURIS | WormBase ParaSite | PRJEB524 |
| <i>Teladorsagia circumcincta</i> | TCIRCU | WormBase ParaSite | PRJNA72569 |
| <i>Tetranychus urticae</i> | TURTI | WormBase ParaSite | PRJEA71041 |
| <i>Thelazia callipaeda</i> | TCALLI | WormBase ParaSite | PRJEB1205 |
| <i>Toxocara canis</i> | TCANIS | WormBase ParaSite | PRJEB533 |
| <i>Trichinella nativa</i> | TNATIV | WormBase ParaSite | PRJNA179527 |
| <i>Trichinella spiralis</i> | TSPIRA | WormBase ParaSite | PRJNA12603 |
| <i>Trichuris muris</i> | TRMURI | WormBase ParaSite | PRJEB126 |
| <i>Trichuris suis</i> | TRSUIS | WormBase ParaSite | PRJNA179528 |
| <i>Wuchereria bancrofti</i> | WBANCR | WormBase ParaSite | PRJEB536 |

Table S3

| Software | Version | Relevant parameters |
|-----------------|----------------|---|
| softWorx | 7.0.0 | |
| Priism | 4.7.1 | |
| OrthoFinder | 2.2.7 | -og |
| MAFFT | 7.407 | --auto |
| IQ-TREE | 1.6.10 | -bb 1000, -bb -m GTR20+G |
| PhyloTreePruner | 20150918 | 35 0.9 u |
| NCBI-BLAST+ | 2.5.0+ | blastp |
| trimAl | v1.4.rev15 | -gt 0.8 -st 0.001 - resoverlap 0.75 - seqoverlap 80 |
| catfasta2phymI | - | -c -f |